Journal of Naval Architecture and Marine Engineering
July, 2026
https://dx.doi.org/10.3329/jname.v23i2.87987 https://www.banglajol.info

SYNERGISTIC EFFECTS OF TRIHYBRID NANOFLUID ON THERMAL PERFORMANCE IN A PARALLEL PLATE HEAT EXCHANGER

Rehena Nasrin[1,]*, Nusrat Jahan Jakia[1], and Yassine El Alami[2]
[1]Department of Mathematics, Bangladesh University of Engineering and Technology, Dhaka-1000, Bangladesh
[2]Laboratory of Electronics, Instrumentation and Energetic, Faculty of Sciences, Chouaïb Doukkali University, B.P 20, El Jadida, Morocco
*rehena@math.buet.ac.bd, jakia.math.buet@gmail.com, yassineelalami97@gmail.com

Abstract:
The study investigates the thermal performance and efficiency of a 3-chambered parallel plate heat exchanger (PPHE) enhanced with an innovative cold tri-hybrid nanofluid. This advanced tri-hybrid nanofluid comprises graphene (G), silver (Ag), and gold (Au) nanoparticles suspended in a 50:50 mixture of distilled water (DW) and ethylene glycol (EG). The tri-hybrid nanofluid is employed in the upper and lower pipes of the heat exchanger, while heated oil flows through the center pipe. Using a numerical approach, the finite element method (FEM) is employed to solve the governing equations and simulate the thermal behavior of the heat exchanger (HE) under various operating conditions. The simulation shows plots of surface velocity, temperature, streamlines, isotherm lines, and pressure, illustrating temperature and velocity changes in the counter-flow heat exchanger. It assesses performance metrics, including heat transfer (HT) efficiency, HT rate per unit pumping power, and the HE performance index, highlighting the benefits of tri-hybrid nanofluids for enhanced HT. The optimized Nusselt number (Nu) shows improvements of approximately 70% and 13% for increasing Reynolds number (Re = 2-50) and nanoparticle concentration (φ = 0-0.03), respectively, indicating enhanced thermal conductivity and HT efficiency with higher nanoparticle concentration. The total pressure drop increases by about 0.76% at φ = 0.01, with Re varying from 2 to 50, indicating a balance between HT and pressure drop. Additionally, the present study demonstrates up to a 20% higher performance index at lower Re values than reported by Hasan et al. (2009), highlighting the effectiveness of the tri-hybrid nanofluid in enhancing HE performance. The findings enhance understanding of advanced nanofluids in industrial HT systems. This research explores the properties of tri-hybrid nanofluids to guide future HE designs and improve energy efficiency in industrial processes.

Keywords: Parallel plate heat exchanger, trihybrid nanofluid, finite element method, thermal performance, heat transfer enhancement.

NOMENCLATURE:

Ag	Silver nanoparticle
Au	Gold nanoparticle
C_p	Specific heat ($Jkg^{-1}K^{-1}$)
CFD	Computational fluid dynamics
Dh	Hydraulic diameter (m)
DW	Distilled water
EG	Ethylene glycol
f	Friction factor
Fc	Synergy number
G	Graphene nanoparticle
H	Pipe height (m)
HE	Heat exchanger
HT	Heat transfer
K	Thermal conductivity ($Wm^{-1}K^{-1}$)
L	Pipe length (m)
MCHS	Microchannel heat sink
N	Pipe number
Nu	Nusselt number
Δp	Pressure dropping (Pa)
p	Pressure ($kgms^{-2}$)
PHE	Plate heat exchanger
PPHE	Parallel plate heat exchanger
Re	Reynolds number
T	Temperature (K)
u, *v*	Velocity (ms^{-1})
W	Pipe width (m)
α	Thermal diffusivity (m^2s^{-1})
μ	Dynamic viscosity (Nsm^{-2})
ε	Thermal efficiency
ρ	Density (kgm^{-3})
η	Performance index
φ	Nanoparticle concentration

Subscript:

co	cold
coin	cold input
coot	cold output
def	definite
ext	extreme

1813-8535 (Print), 2070-8998 (Online) Received on: Feb., 2026

ho	hot	in	input
hoin	hot input	thnf	tri-hybrid nanofluid
hoot	hot output	s	solid surface

1. Introduction

The exploration of nanofluids has significantly advanced thermal management, particularly in heat exchangers. This section focuses on developing and applying tri-hybrid nanofluids, precisely the combination of graphene, silver, and gold nanoparticles, in optimizing heat exchanger performance. This section reviews recent studies, highlights key advancements, and addresses the challenges of using these cutting-edge fluids to enhance HT efficiency in HEs.

HEs are widely used in many manufacturing processes to transport heat between two fluids. In the studies of Peng et al. (1995), Hasan et al. (2009), and Tiwari et al. (2014), thin steel plates separating the pipes served as effective heat-conducting media and maintained operational integrity. Ordonez and Bejan (2000) demonstrated that the main architectural features of a counterflow heat exchanger can be optimized to minimize irreversibility while satisfying a volume constraint. It shows that the optimal design is robust to variations in the channel spacing ratio, HT area, and the capacity ratio of the two streams. Galeazzo et al. (2006) developed a computational fluid dynamics (CFD) virtual prototype of a four-channel plate heat exchanger and tested parallel and series flow arrangements. CFD results closely matched experimental data, particularly for the series arrangement, accounting for flow distribution and maldistribution. Hong and Cheng (2009) studied velocity and temperature distributions, examined the impact of strip fins, and proposed design guidelines for strip-fin microchannel heat sinks (MCHS) for microelectronic freezing. Gherasim et al. (2011) experimentally investigated hydrodynamic and thermal fields in a chevron-type plate heat exchanger. Results show intermediate friction and Nusselt numbers, influenced by geometry and configuration, with temperature distributions revealing isotherm distortions due to smooth passages along plate edges.

Hasan (2011) investigated the flow and HT of microencapsulated phase change material (MEPCM) suspension in a counterflow microchannel heat exchanger (CFMCHE). Using MEPCM suspensions as coolants enhances thermal performance but increases pressure drop, thereby affecting overall performance compared to pure fluids. Sundar et al. (2014) found that dispersing Al_2O_3 nanoparticles in EG-W mixtures increases thermal conductivity and viscosity with higher volume concentrations and temperatures. The 20:80% EG-W mixture showed the greatest increase in thermal conductivity, while the 60:40% EG-W mixture exhibited the greatest increase in viscosity. Guo et al. (2015) explained that designing optimal multi-stream plate-fin heat exchangers is complex due to the many combinations of standardized fin geometries. This work proposes a new design algorithm that treats basic fin geometries as continuous variables, optimizing thermal-hydraulic performance and minimizing the heat exchanger's total volume. Barjegarian et al. (2016) investigated the effects of TiO_2-water (titanium oxide-water) nanofluid on HT and pressure drop in a brazed plate heat exchanger under turbulent flow. Results showed significant increases in convective and overall HT coefficients with higher nanoparticle concentrations, accompanied by negligible increases in pressure drop. Arasteh et al. (2019) examined HT in a sinusoidal parallel-plate heat exchanger with metal foam. Results show a 19.2% increase in HT rate and a performance evaluation criterion (PEC) of 1.171, highlighting the effectiveness of metal foam in improving performance with minimal impact on pumping power.

Wang et al. (2020) presented a novel double-layered MCHS design that accounted for pressure drop, coolant velocity, and mixing effects. Their MCHS incorporated porous vertical ribs with sinusoidal microchannels, thereby providing a larger cooling volume than earlier models. Elsaid et al. (2021) highlighted that graphene-based nanofluids significantly enhance thermal conductivity, achieving up to a 40% increase, making them efficient HT fluids. It also addresses stability, density, cost, viscosity, and environmental challenges, providing mitigation recommendations. Zheng et al. (2021) studied cone-column MCHS and found it to have better HT than circular microchannels, with improved flow, lower base temperatures, and advanced average Nusselt numbers, making it suitable for high-power electronic cooling. Zhu et al. (2021) optimized microchannel sidewall geometries, finding that water-droplet-grooved minimized pressure drop and improved HT. Plate heat exchangers (PHEs) are particularly popular due to their high HT efficiency, compact design, and ease of maintenance, making them suitable for a wide range of applications across industries (Li et al. (2021), Marra et al. (2021), Kikic et al. (2021), and Oliveira et al. (2021)). Zahan et al. (2022) analyzed ternary nanoparticles' impact in base-fluid mixtures using a convergent-divergent nozzle, focusing on laminar flow characteristics, and found an optimum HT rate when using ethylene glycol-cobalt-silver-zinc nanofluid.

Reddy et al. (2024a, b) investigated tri-composite and Casson-Maxwell nanofluids on porous surfaces, applying non-Fourier heat conduction principles. Sohail et al. (2023, 2024a, b, 2025) conducted a numerical analysis of both two- and three-dimensional axisymmetric steady and unsteady cases, encompassing phenomena such as radiation, viscous dissipation, heat generation, magnetohydrodynamic effects, entropy generation, and a four-phase fluid temperature jump. Their study utilized water-based hybrid and tetra-hybrid nanofluids flow to enhance thermal performance on radially stretched surfaces, a spinning sphere, and Darcy-Forchheimer squeezed flows between two parallel rotating disks. Alatawi et al. (2025a, b) conducted CFD analyses using various physical models, including HE and heat sink models, with suitable boundary conditions, employing finite-difference and FEM methods. The authors addressed boundary-layer analysis and heat-transport modelling. Jahan et al. (2025a, b, 2026) conducted a sensitivity analysis of performance criteria for a crossflow microchannel HE. They used response surface methodology and predictive ANN analysis to study the hydrothermal and entropy characteristics of a corrugated HE with tetra-hybrid nanofluid, as well as thermal enhancement with a ternary-hybrid nanofluid in a two-layered configuration. Mebarek-Oudina et al. (2024, 2025a, b, 2026) studied the optimization of thermal performance in shell-and-tube heat exchangers using tri-hybridized nanofluids. Their research included numerical analysis of turbulent convection, heat transfer with entropy generation in a partially filled, corrugated heat exchanger with a porous medium, improving thermodynamic irreversibility and heat transfer with rotating graphene oxide–water nanofluids on a stretching surface, and an experimental and machine-learning study of ZnO nanofluid flow in a triangular-absorber parabolic collector.

The literature review clearly indicates that there is a research gap regarding tri-hybrid nanofluid based on (50:50%) DW-EG mixtures in the PPHE system. This research aims to investigate the HT enhancement of a PPHE using a trihybrid nanofluid based on a water-ethylene glycol mixture. It intends to investigate the effects of different concentrations of G-Ag-Au nanoparticles on the system's HT rate and pressure drop. Furthermore, optimizing the PPHE design for maximum thermal efficiency is the primary goal of this thesis.

1.1 Objectives:

- Investigating the impact of different nanoparticle types and concentrations on the HT rate in PPHE.
- Studying the effect of operational parameters, such as the Reynolds number and nanoparticle concentration, on the enhancement of HT rate using tri-hybrid nanofluid.
- Selecting optimum flow conditions for PPHE heat transfer enhancement using nanofluid.
- Improving HT rates in PPHE by applying tri-hybrid nanofluid.

1.2 Novelties:

This research presents, for the first time, a numerical analysis of a three-chambered parallel-plate heat exchanger using a graphene–silver–gold (G–Ag–Au) tri-hybrid nanofluid in a water–ethylene glycol mixture. The innovation lies in integrating an advanced tri-hybrid nanofluid with a three-channel heat exchanger design, supported by a comprehensive FEM-based thermal-hydraulic analysis. The system achieves significant improvements in heat-transfer efficiency with only a marginal increase in pressure drop and exceeds the performance of previously documented hybrid nanofluid heat exchangers by up to 20%, underscoring its potential for future industrial thermal management applications.

2. Physical Model

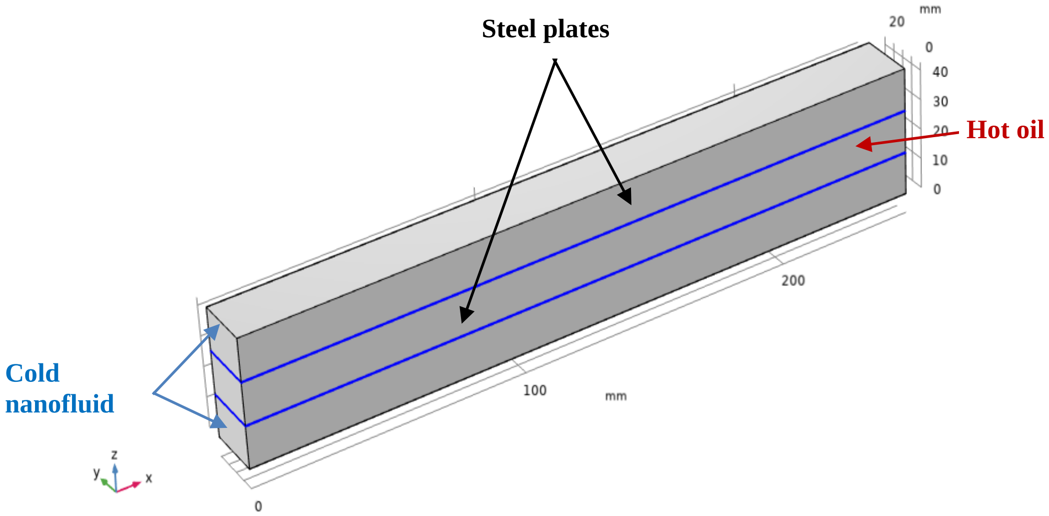

Figure 1: Model geometry of plate heat exchanger (Zahan et al. (2025)).

The physical model of the PPHE shown in Figure 1 consists of three pipes and two parallel plates. The width, height, and thickness of the pipes are 20.20 mm, 14.10 mm, and 0.10 mm, respectively. The model is assembled from three pipes, each topped and bottomed with two 0.20 mm-thick steel plates, and has the same dimensions as the pipes. For the cold tri-hybrid nanofluid, the flow configuration consists of one inlet (bottom) and two outlets (top and bottom), whereas for hot oil, it has only an inlet (top) and an outlet, as shown in Figure 1. The tri-hybrid nanoparticles are G-Ag-Au, based on a DW:EG (50:50) fluid mixture and an oil with defined thermophysical properties, as shown in Table 1. The cold tri-hybrid nanofluid with an inlet velocity of 0.005 feed. The hot oil flows through the central channel at 320 K.

3. Mathematical Modeling

Following the Boussinesq approximation, the governing equations and boundary conditions are provided by Jahan et al. (2025):

$$\begin{cases} \dfrac{\partial u}{\partial x}+\dfrac{\partial v}{\partial y}+\dfrac{\partial w}{\partial z}=0 \\ u\dfrac{\partial u}{\partial x}+v\dfrac{\partial u}{\partial y}+w\dfrac{\partial u}{\partial z}=-\dfrac{\partial p}{\partial x}+\dfrac{\mu_{thnf}}{\rho_{thnf}}\left(\dfrac{\partial^2 u}{\partial x^2}+\dfrac{\partial^2 u}{\partial y^2}+\dfrac{\partial^2 u}{\partial z^2}\right) \\ u\dfrac{\partial v}{\partial x}+v\dfrac{\partial v}{\partial y}+w\dfrac{\partial v}{\partial z}=-\dfrac{\partial p}{\partial y}+\dfrac{\mu_{thnf}}{\rho_{thnf}}\left(\dfrac{\partial^2 v}{\partial x^2}+\dfrac{\partial^2 v}{\partial y^2}+\dfrac{\partial^2 v}{\partial z^2}\right) \\ u\dfrac{\partial w}{\partial x}+v\dfrac{\partial w}{\partial y}+w\dfrac{\partial w}{\partial z}=-\dfrac{\partial p}{\partial z}+\dfrac{\mu_{thnf}}{\rho_{thnf}}\left(\dfrac{\partial^2 w}{\partial x^2}+\dfrac{\partial^2 w}{\partial y^2}+\dfrac{\partial^2 w}{\partial z^2}\right) \\ u\dfrac{\partial T_{thnf}}{\partial x}+v\dfrac{\partial T_{thnf}}{\partial y}+w\dfrac{\partial T_{thnf}}{\partial z}=\dfrac{\alpha_{thnf}}{\alpha_{bf}}\left(\dfrac{\partial^2 T}{\partial x^2}+\dfrac{\partial^2 T}{\partial y^2}+\dfrac{\partial^2 T}{\partial z^2}\right) \\ \dfrac{\partial^2 T_s}{\partial x^2}+\dfrac{\partial^2 T_s}{\partial y^2}+\dfrac{\partial^2 T_s}{\partial z^2}=0 \end{cases} \tag{1}$$

3.1 Boundary conditions

Inlet temperature T = 300 K and inlet velocity u_{in} m/s are present at the top-bottom pipes.

The temperature in the middle hot channel is T = 320 K, and the inlet velocity is $-u_{in}$ m/s.

Every other solid wall, $u=v=w=0$

To maintain equal source and destination temperatures, the model's top-bottom layers are kept at temperature, $\Delta T=0$ K.

The solid channel is kept insulated on both of its vertical surfaces.

All outlets, $P=0$.

The boundaries of solid-fluid, $u=v=w=0$, $k_s\frac{\partial T_s}{\partial n}=k_{thnf}\frac{\partial T_{thnf}}{\partial n}$, $T_s=T_{thnf}$

3.2 Corresponding expressions

- Reynolds number, $Re==\frac{\rho_{bf}\,u_{in}D_h}{\mu_{bf}}$ (2)
- Hydraulic diameter, $D_h(m)=\frac{2LW}{L+W}$, L = 0.02 m, W = 0.014 m (3)
- Prandtl number, $Pr=\left(\frac{\mu\,Cp}{k}\right)_{thnf}$ (4)
- Heat Transfer at hot oil inlet (Jahan et al. (2025a)), $Nu=-\left(\frac{k_{thnf}}{k_{bf}}\right)\int_0^s\frac{D_h}{(T_{ho}-T_{co})}\frac{\partial T}{\partial n}ds$ (5)
- Pressure drop (Jahan et al. (2026)), $\Delta p=\Delta P_{co}+\Delta P_{ho}=(P_{coin}-P_{coot})+(P_{hoin}-P_{hoot})$ (6)
- Friction factor, $f=\frac{\Delta p\,D_h}{2\rho_{thnf}\,L\,u_{thnf}^2}$ (7)
- Synergy number, $Fc=\frac{Nu}{Re\,Pr}$ (8)
- Volumetric flow rate (Jahan et al. (2025b)), $Q(\text{Pa. m}^3/\text{s})=N_{ch}A_{ch}u_{in}$ (9)
- Total pumping power (Jahan et al. (2025)), $P_{pu}(\text{m}^3/\text{s})=Q_{ho}\Delta P_{ho}+Q_{co}\Delta P_{co}$ (10)
- Thermal effectiveness (Zahan et al. (2025)), $\varepsilon=\frac{q_{def}}{q_{ext}}$ (11)
- Performance index (thermal) (Hasan (2009), $\eta^*(\frac{1}{Pa})=\frac{\varepsilon}{\Delta P}$ (12)
- Performance index (hydraulic) (Hasan (2009), $\eta=\frac{q}{P_{pu}}$ (13)

where, N_{ch} is pipe number, $q_{ext} = mC_p(T_{hoin} - T_{coin})$, and $q_{def} = (mC_p)_{ho}(T_{hoin} - T_{hoot}) = (mC_p)_{co}(T_{coin} - T_{coot})$, are extreme and definite thermal transfer, respectively.

The performance index links thermal and hydrodynamic performance to indicate the overall exchanger performance.

3.3 Properties

Thermo-physical properties depend on the physical characteristics of materials and base fluids and vary with temperature and pressure, while the chemical nature is maintained. This research examines these properties at room temperature for both nanoparticles and base fluids. The thermophysical properties are detailed in Tables 1 and 2 and serve as the basis for the simulation parameters.

Table 1: Properties (Sundar et al. (2014), Li et al. (2021), Elsaida et al. (2021), Zahan et al. (2022), Jahan et al. (2025)).

	Thermal conductivity ($Wm^{-1}K^{-1}$)	**Density (kgm^{-3})**	**Viscosity (Nsm^{-2})**	**Specific heat ($Jkg^{-1}K^{-1}$)**
DW:EG (50:50)	0.3712	1110	3.21×10^{-3}	3354
G	4000	2270	-----	509
Ag	429	10400	-----	0.234
Au	320	19300	-----	129.1
Oil	1.450	876.0	0.21770	1964.0
Steel	44.50	7850.0	---	475.0

Table 2: Effective properties (Zahan et al. (2022, 2025), Jahan et al. (2026)).

Properties	**Expression**
Density	$\rho_{thnf} = (1-\phi)\rho_{bf} + \phi_G\rho_G + \phi_{Ag}\rho_{Ag} + \phi_{Au}\rho_{Au}$
Viscosity of Brinkman model (1952)	$\mu_{thnf} = \dfrac{\mu_{bf}}{(1-\phi_G-\phi_{Ag-}\phi_{Au})^{2.5}}$
Heat capacitance	$(\rho C_p)_{thnf} = (1-\phi)(\rho C_p)_{bf} + \phi_G(\rho C_p)_G + \phi_{Ag}(\rho C_p)_{Ag} + \phi_{Au}(\rho C_p)_{Au}$
Specific heat	$C_{pthnf} = \dfrac{(1-\phi)(\rho C_p)_{bf} + \phi_G(\rho C_p)_G + \phi_{Ag}(\rho C_p)_{Ag} + \phi_{Au}(\rho C_p)_{Au}}{(1-\phi)\rho_{bf} + \phi_G\rho_G + \phi_{Ag}\rho_{Ag} + \phi_{Au}\rho_{Au}}$
Thermal conductivity of Maxwell Garnett model (1904)	$k_{thnf} = k_{bf}\dfrac{\left(\dfrac{\phi_G k_G + \phi_{Ag}k_{Ag+}\phi_{Au}k_{Au}}{\phi}\right) + 2k_{bf} - 2\left(k_{bf} - \dfrac{\phi_G k_G + \phi_{Ag}k_{Ag+}\phi_{Au}k_{Au}}{\phi}\right)\phi}{\left(\dfrac{\phi_G k_G + \phi_{Ag}k_{Ag+}\phi_{Au}k_{Au}}{\phi}\right) + 2\,k_{bf} + \left(k_{bf} - \dfrac{\phi_G k_G + \phi_{Ag}k_{Ag+}\phi_{Au}k_{Au}}{\phi}\right)\phi}$

The nanoparticles' solid fraction, $\phi = \phi_G + \phi_{Ag} + \phi_{Au}$.

3.4 Nanoparticle dispersion stability

- ❖ The DW:EG (=50:50) mixture-based G–Ag–Au tri-hybrid nanofluid is assumed to be a stable, homogeneous, single-phase suspension throughout the computational domain.
- ❖ Nanoparticle agglomeration, sedimentation, and phase separation are neglected, and thermal equilibrium between the nanoparticles and the base fluid is maintained.
- ❖ The effective thermophysical properties are evaluated using established mixture relations and are assumed to remain constant at a specified nanoparticle volume fraction, thereby ensuring stable nanoparticle dispersion during heat transfer.

4. Numerical Computation

This study utilizes a comprehensive numerical framework to evaluate the thermal criteria of a three-chambered PPHE enhanced with a trihybrid nanofluid comprising a 50:50 mixture of DW and EG. This approach is vital for precisely analyzing the multifaceted connections between fluid flow and HT within the HE. To ensure the precision of our simulations, we applied advanced numerical analysis techniques to generate a high-quality mesh tailored to the heat exchanger geometry. The resulting mesh, formed from rectangular or square elements, closely aligns with the channel design, providing an optimal basis for accurate simulations. For numerical computations, FEM with the Galerkin weighted residual approach Zienkiewicz and Taylor (1991) provides reliable, stable solutions, thereby enhancing the overall accuracy of thermal performance predictions.

4.1 Assumptions in FEM modeling

- The computational domain is represented by non-uniform finite element meshes consisting of six-noded triangular and ten-noded tetrahedral elements.
- The dependent variables are approximated with polynomial shape functions, while pressure is interpolated with a lower-order approximation to satisfy the continuity constraint.
- The Galerkin weighted residual method is used to derive the weak form of the governing equations, and Gauss quadrature is used for numerical integration.
- Nonlinearities are treated with Newton–Raphson iterations, and the resulting linear algebraic system is solved by triangular factorization.
- The numerical solution is considered converged when the residual norm falls below 10^{-4}.

4.2 Mesh creation with grid check

Figures 2(a-b) display the mesh generation for the PPHE.

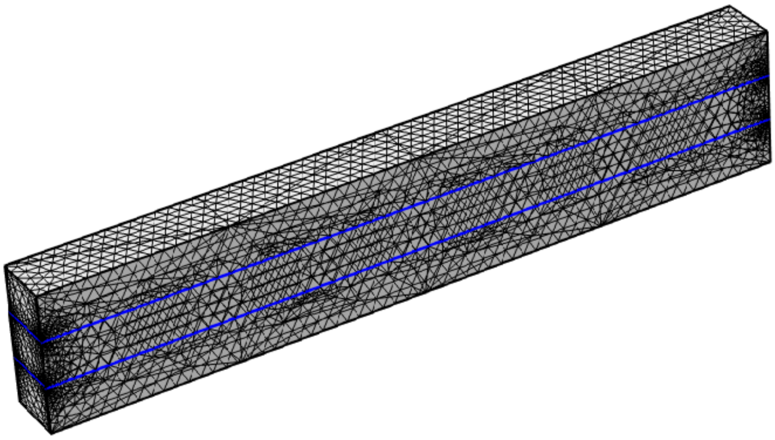

(a)

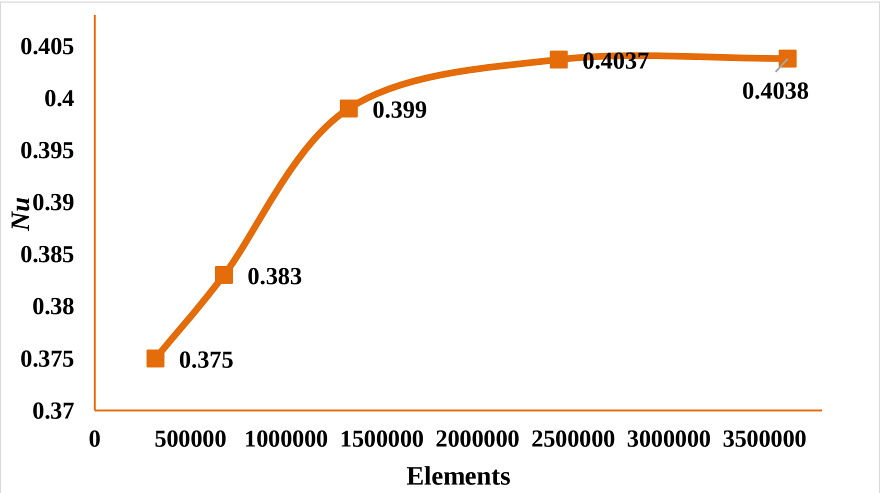

(b)

Figure 2: (a) Mesh generation, and (b) grid test for Re = 50, $\phi = 0.01$

4.3 Model validation

Table 3 provides a comparative validation of the cold fluid outlet temperature for several nanoparticles, including titanium dioxide, silicon dioxide, aluminum oxide, and silver. The findings of Mohammed et al. (2011) are compared with the current study to assess the accuracy of the computational analysis. The validation is performed for a single-layer parallel-flow microchannel heat exchanger (MCHE) featuring 25 cold and hot channels under standard conditions: $100 < Re < 800$, $2\% < \phi < 10\%$ and inlet temperatures of 303K for hot and 293K for cold. In this investigation, the cold channel outlet for each nanofluid exhibits significant agreement with the findings of Mohammed et al. (2011), with error percentages ranging from 0.02% to 0.12%. The minor variations validate the dependability and precision of the current numerical model in forecasting nanofluid heat transfer performance.

Table 3: The cold fluid outlet temperature (K) for different nanoparticles.

Cold fluid	Mohammed et al. (2011)	Present study	Error (%)
Water	297.34	297.70	0.12
Aluminum oxide	297.44	297.50	0.02
Silicon dioxide	297.36	297.45	0.03
Silver	297.77	297.66	0.04
Titanium dioxide	297.45	297.39	0.02

5. Results and Discussion

The numerical analysis of a parallel-plate HE reveals several key insights into its thermal and fluid-dynamic behavior. The results comprehensively examine surface velocity-temperature, streamlines, isotherms, and the overall thermal transfer efficiency. Critical parameters, including pressure drop, pumping power, friction factor, and synergy number, are thoroughly analyzed to assess the collaboration between flow characteristics and HT efficiency. The contour plots provide a clear visualization of these phenomena. In the streamline plots, the lines effectively illustrate the flow patterns within the PPHE, while the accompanying color graphs depict the velocity surface. Similarly, the isothermal contour plots show the isotherm lines, highlighting temperature gradients, while the color maps display the temperature distribution across the surface. These visual and quantitative analyses provide a detailed understanding of the HE's performance characteristics, demonstrating how the innovative tri-hybrid nanofluid influences key factors, including HT rate and flow resistance. The results not only confirm the model's effectiveness but also offer valuable insights for enhancing the design and operation of HEs in industrial settings.

5.1 Velocity impact

This study examines the effect of cold tri-hybrid nanofluid inlet velocity in terms of Reynolds number (Re = 2-50) on the thermal characteristics of a three-chambered PPHE with a fixed nanoparticle volume fraction ϕ = 0.01. The associated velocity (u_{in}) values are 0.00033, 0.000414, 0.00066, 0.00083, 0.0017, 0.0033, 0.0049, 0.0066, and 0.0083 m/s for the Reynolds numbers of 2, 3, 4, 5, 10, 20, 30, 40, and 50, respectively. The results are analyzed through surface temperature, isothermal contours, velocity streamlines, and pressure iso-surfaces. As Re increases, turbulence within the flow increases, leading to improved mixing and enhanced heat transfer, significantly increasing the overall HT rate. Higher Re values create more uniform temperature distributions across the heat exchanger, reducing thermal gradients and hotspots, and promoting efficient heat dissipation. Higher Re enhances HT but increases pressure drop due to higher frictional losses, necessitating a balance between achieving optimal HT and managing the required pumping power. With increasing Re, the velocity profiles and streamlines become more chaotic and irregular, improving convective HT and resulting in higher pressure losses. The performance index (η), which accounts for HT efficiency and pressure drop, varies with Re. Identifying an optimal Re is essential for maximizing HT while maintaining acceptable pressure drops. These findings highlight the importance of selecting appropriate Reynolds numbers to optimize HE performance, balancing enhanced HT with manageable pressure drops.

5.1.1 Surface temperature

Figure 3 describes the surface temperature plot of the three-layered PPHE using the tri-hybrid nanofluid, which exhibits significant variations with different Reynolds numbers, maintaining a constant nanoparticle volume fraction $\varphi = 0.01$. At low Reynolds numbers (Re = 2), the surface temperature profiles are less uniform, with noticeable thermal gradients and warmer color profiles indicating less efficient HT. Rising Re to 3, 4, and 5, the profiles show improved uniformity, with the color gradients becoming more subdued, reflecting better heat dissipation. At moderate Reynolds numbers (*Re* = 10 and 20), the surface temperature distribution becomes

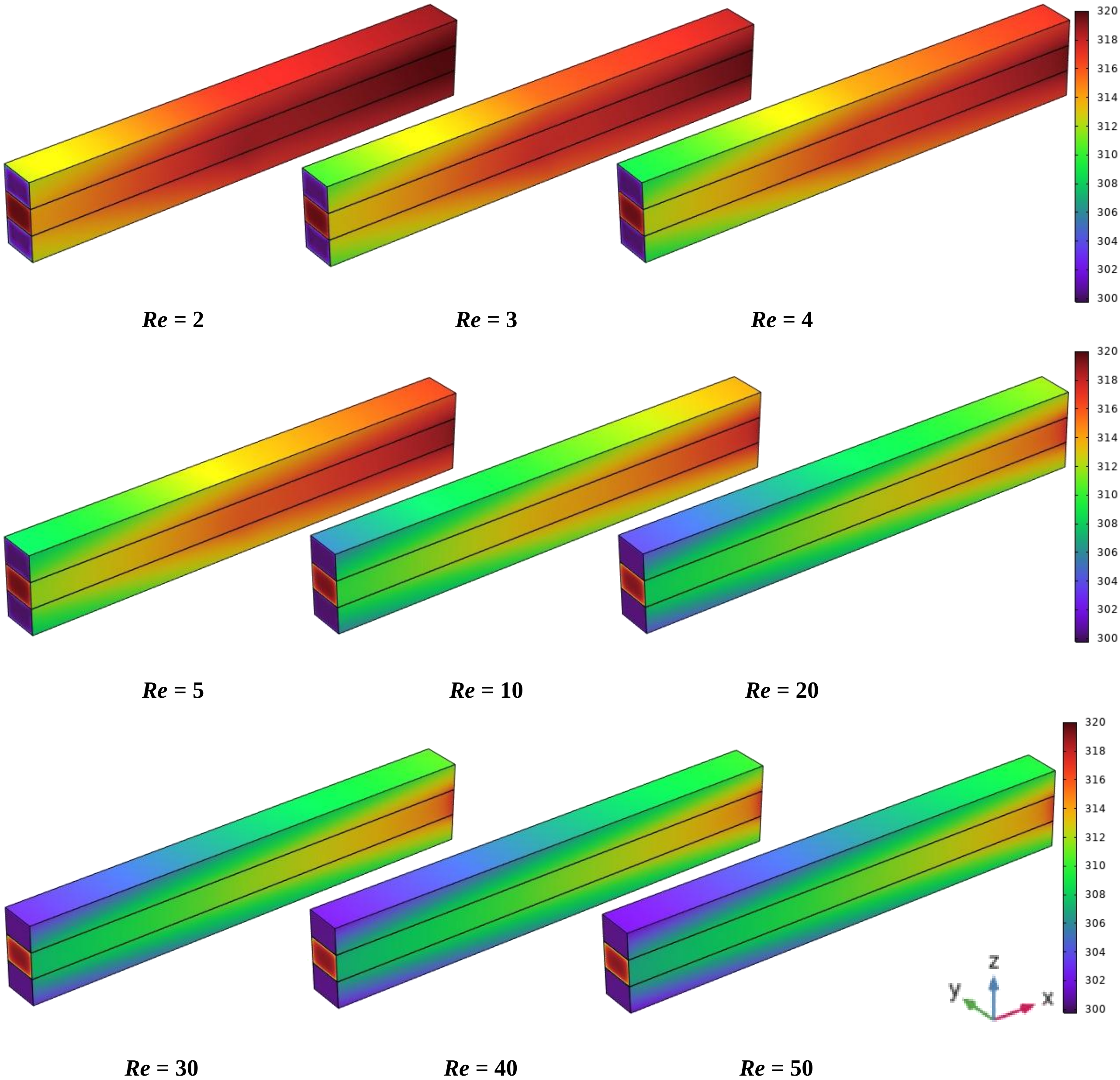

Figure 3: The surface temperature for different Reynolds numbers when ϕ = 1%

significantly more uniform, with cooler and more consistent color profiles indicating enhanced convective HT and reduced thermal gradients. At higher Reynolds numbers (*Re* = 30, 40, and 50), the surface temperature profiles are the most uniform, with the coolest and most consistent color profiles indicating the highest HT efficiency. The transition in profile colors from warmer to cooler tones as the Reynolds number increases highlights enhanced turbulence and mixing within the heat exchanger, leading to superior thermal performance and optimal heat dissipation.

5.1.2 Isothermal contour

Figure 4 shows the effect of varying Reynolds numbers on isothermal contours when $\varphi = 0.01$. At low Reynolds numbers (*Re* = 2, 3, 4, 5), contours are widely spaced and show transparent temperature gradients, indicating an uneven heat distribution. Contours tighten at moderate *Re* (10 and 20), showing enhanced convective heat transfer. At high *Re* (30, 40, and 50), contours indicate optimal HT efficiency. This transition underscores enhanced turbulence and mixing, leading to superior thermal performance.

5.1.3 Streamlines of velocity magnitude

When $\varphi = 0.01$, the effect of varying Reynolds numbers on velocity streamlines is shown in Figure 5. At lower Reynolds numbers (*Re* = 2, 3, 4, 5), the streamlines are more dispersed and slower, indicating inefficient flow. As the Reynolds number increases to moderate values (10 and 20), the streamlines become more organized, showing improved flow dynamics. At higher Reynolds numbers (Re = 30, 40, and 50), the streamlines are closely aligned with the faster velocities, indicating optimal flow efficiency. This progression highlights increased turbulence and mixing, resulting in superior overall performance.

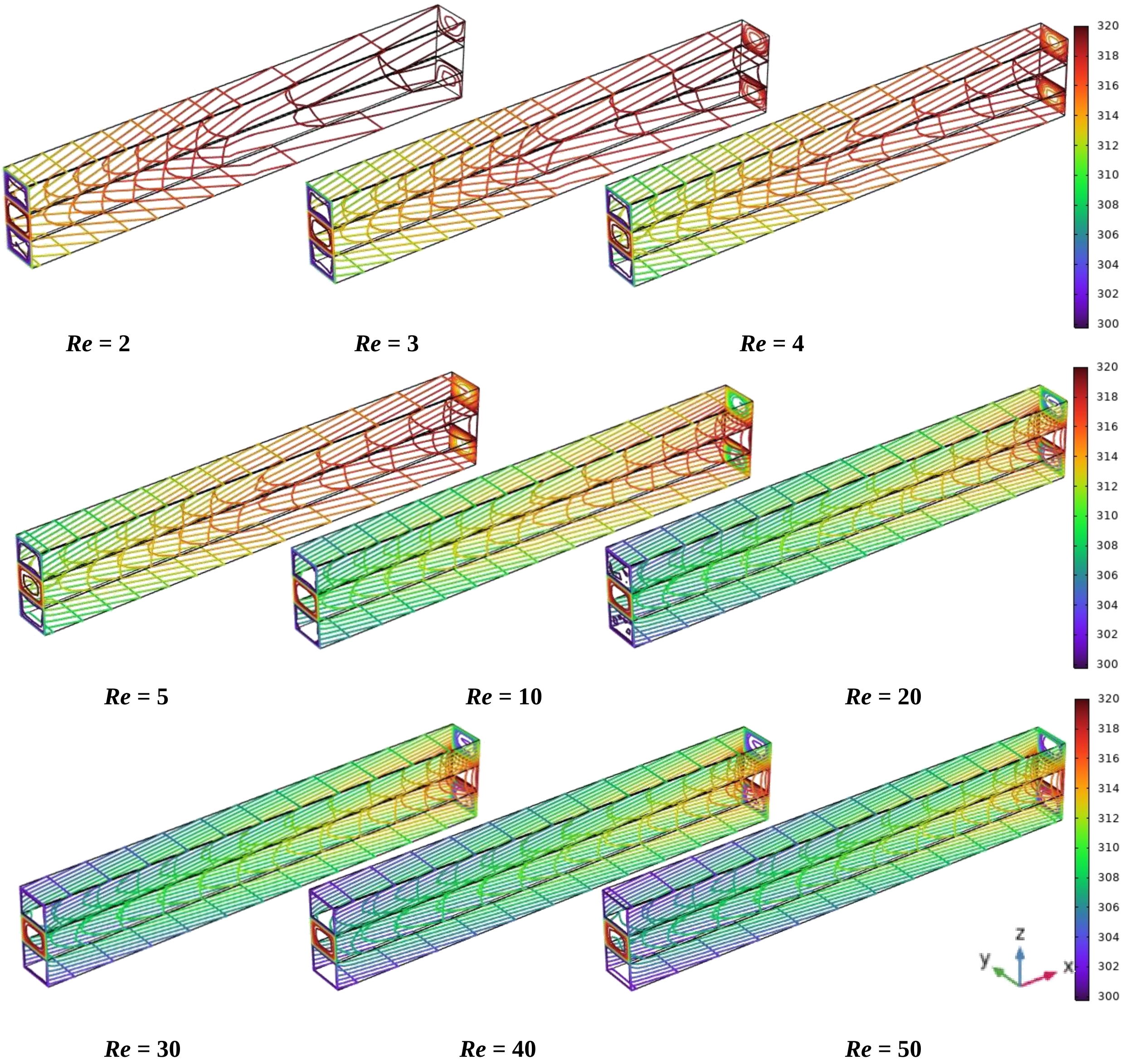

Figure 4: Isothermal contour at different Re numbers when $\varphi = 1\%$.

5.1.4 Iso-surfaces for pressure

The pressure isosurface profiles vary significantly with Reynolds numbers, shown in Figure 6. At lower Reynolds numbers, the isosurface is uneven, indicating significant pressure drops. The isosurfaces smooth out as the Re increases to moderate levels (10 and 20), showing more stable pressure distributions. The isosurfaces are uniform at high Re (30, 40, 50), indicating minimal pressure drops and optimal efficiency. This trend demonstrates that higher Reynolds numbers improve pressure management and system performance.

5.2 Volume concentration impact

Figure 7 displays that the solid volume fraction (ϕ) plays a crucial role in determining the thermal and flow characteristics of the heat exchanger, especially at a constant Reynolds number ($Re = 3$). The nanoparticle volume fraction is limited to 3% to balance thermal enhancement and hydraulic performance. Increasing the solid fraction improves heat transfer but raises viscosity, pressure drop, and the risk of agglomeration. Low concentrations maintain stability and model validity. Thus, 3% is chosen for practicality, reliability, and realistic operation. Variations in φ can significantly influence heat transfer, fluid flow, and pressure distribution within the system. These changes become particularly evident, demonstrating how nanoparticle concentration in the fluid can enhance or hinder the heat exchanger's effectiveness.

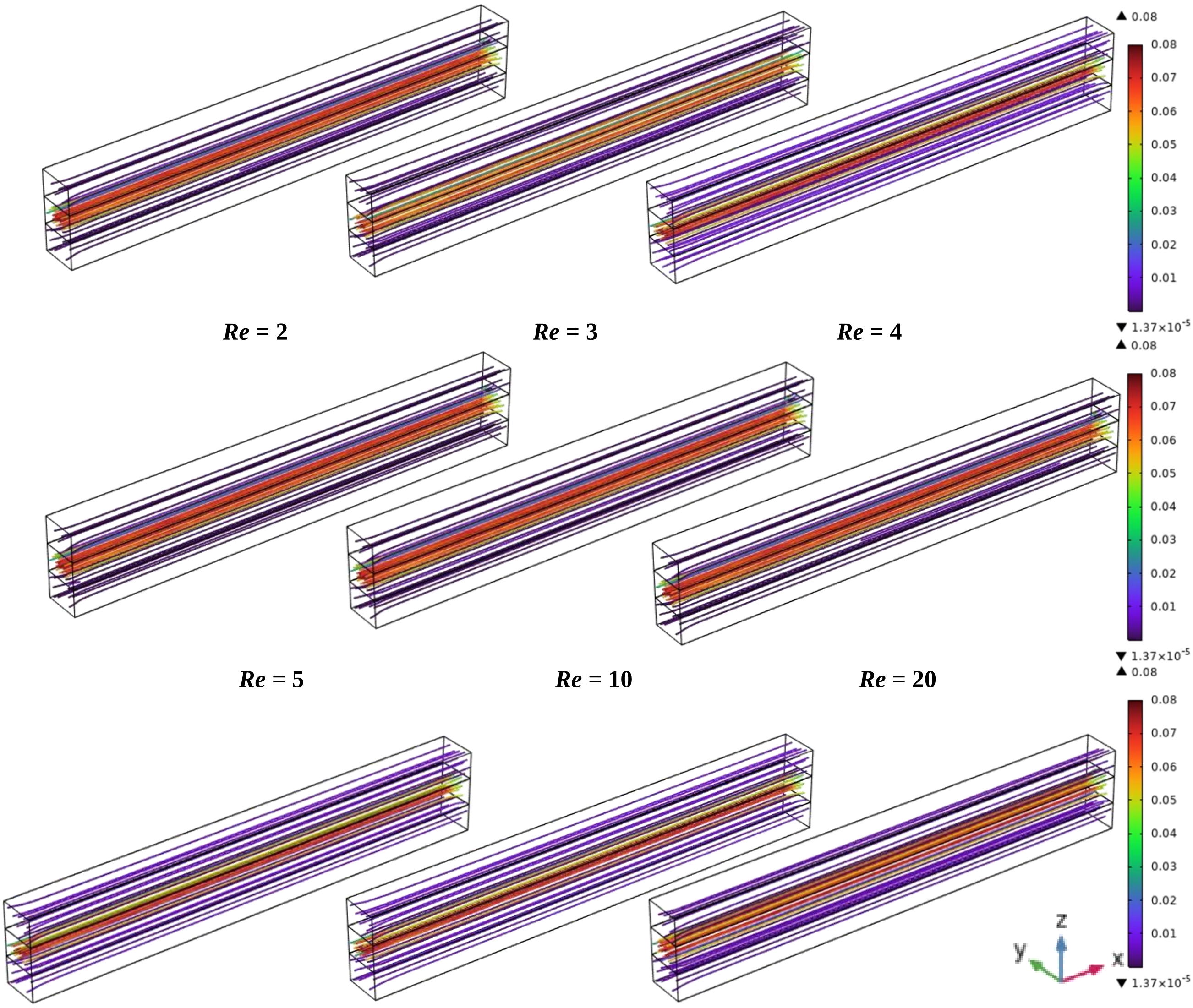

Re **= 2** ***Re*** **= 3** ***Re*** **= 4**

Re **= 5** ***Re*** **= 10** ***Re*** **= 20**

Re **= 30** ***Re*** **= 40** ***Re*** **= 50**

Figure 5: Streamline of velocity magnitude at different *Re* numbers when $\varphi = 1\%$.

Figure 7(a) shows that at $\varphi = 0.001$, the isosurface temperature shows minimal enhancement, indicating essential heat transfer (Figure 7(a)). Increasing φ to 0.005 and 0.015 results in a more uniform, higher-temperature isosurface, reflecting improved thermal conductivity and better heat transfer. At higher volume fractions (φ is 0.02 and 0.03), the iso-surface temperature distribution becomes even more uniform, indicating optimal heat transfer efficiency.

At $\varphi = 0.001$, the velocity magnitude (Figure 7(b)) is relatively low, indicating less momentum transfer (Figure 7(b)). As φ increases to 0.005 and 0.015, the velocity magnitude improves, showing better fluid flow and enhanced momentum transfer. Higher solid volume fractions lead to higher velocity magnitudes, reflecting optimal fluid flow and increased turbulence.

Again, at a lower value of φ, the pressure profile shows significant pressure drops, indicating inefficiencies (Figure 7(c)). The pressure profile smoothens at a moderate value of φ, showing more stable pressure distributions and reduced pressure drops. The pressure profile becomes very uniform at volume concentrations of 0.02 and 0.03, indicating minimal pressure drops and enhanced pressure management.

Figure 7(a-c) effectively illustrates the impact of varying nanoparticle concentrations on the performance of the heat exchanger, emphasizing how increasing the solid volume fraction φ is 0.02 and 0.03 from 0.001 to 0.03, enhances the thermal and flow characteristics, leading to improved heat transfer, better fluid flow, and more efficient pressure management.

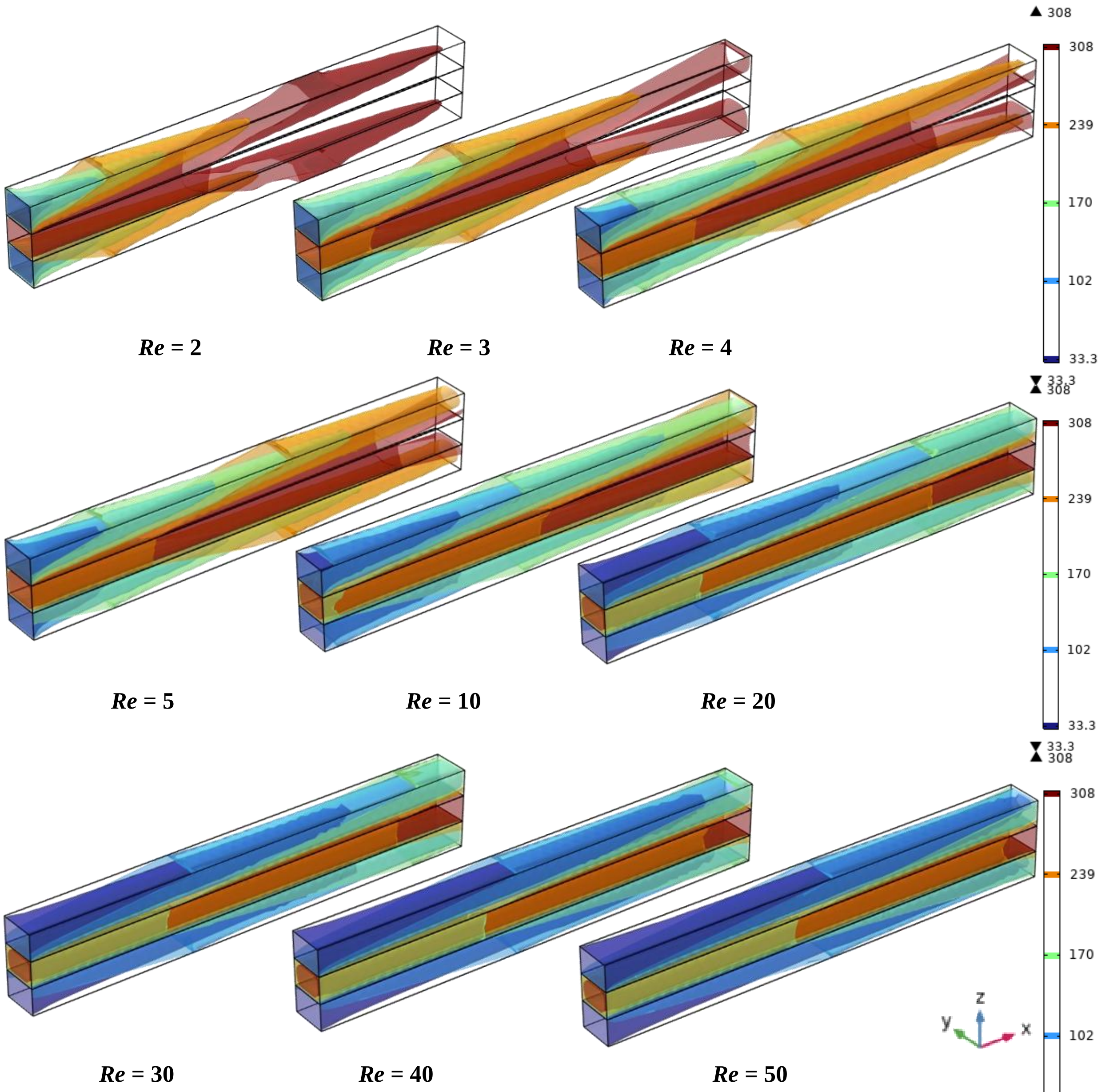

Figure 6: Isosurface profiles for pressure at different *Re* when φ = 1%

5.3 Effect of Nusselt number

The average Nusselt number is critical for evaluating convective heat transfer efficiency in the heat exchanger. An increase in the Nusselt number indicates enhanced heat transfer performance, reflecting a higher convective heat transfer rate relative to conduction. This directly impacts the system's overall thermal efficiency, making it a key parameter in optimizing heat exchanger design. In this study, the mean Nusselt number is calculated by Equation (5).

For different Reynolds numbers:

This graph in Figure 8(a) shows This graph illustrates the variation of the average Nusselt number (*Nu*) concerning the Reynolds number (*Re*) for the tri-hybrid nanofluid (comprising graphene (G), silver (Ag), and gold (Au) nanoparticles) suspended in a 50:50 mixture of distilled water (DW) and ethylene glycol (EG). As *Re* increases, *Nu* also increases, indicating enhanced heat transfer with higher flow rates. *Nu* increases rapidly at low Re (below 10), indicating significant sensitivity to flow changes. Beyond *Re* of 10, the increase in *Nu* becomes more gradual, reflecting a stabilization in heat transfer efficiency. The graph highlights the superior thermal performance of the tri-hybrid nanofluid, demonstrating its potential for improving heat exchanger efficiency in industrial applications. Overall, the graph validates the tri-hybrid nanofluid's effectiveness in enhancing heat transfer performance in the heat exchanger, supporting its potential application in advanced, energy-efficient technologies and industrial processes.

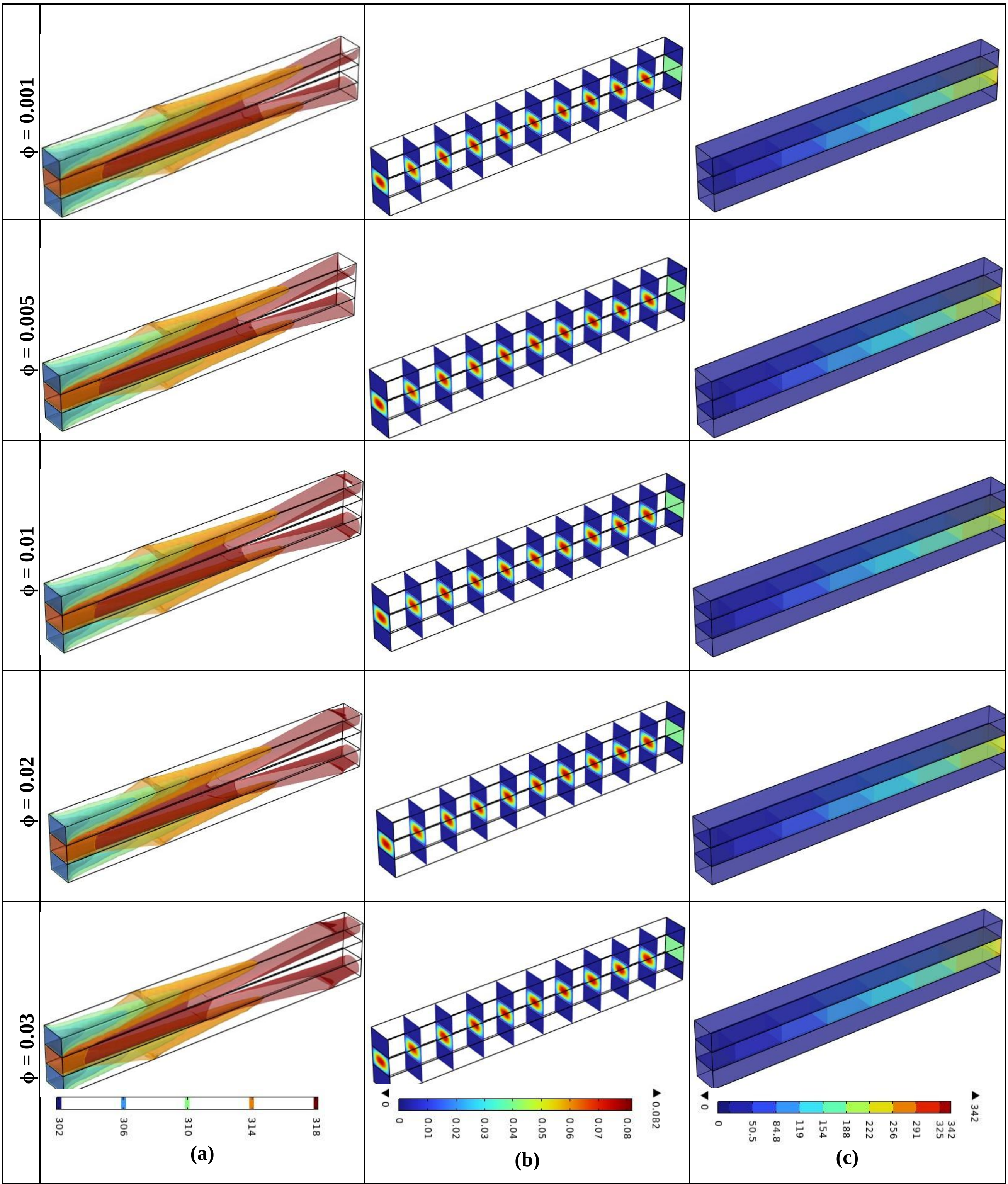

Figure 7: Effect of ϕ with *Re* = 3 on (a) iso-surface temperature, (b) velocity magnitude, and (c) surface pressure

For values of solid volume fraction:

Graph 8(b) demonstrates the effect of nanoparticle volume fraction (φ) on the average Nusselt number (*Nu*) for the tri-hybrid nanofluid used in the heat exchanger. The superior thermal conductivity of the G–Ag–Au tri-hybrid nanofluid (DW:EG = 50:50) stems from synergistic interactions among nanoparticles, which form interconnected networks, reduce interfacial resistance, and enhance micro-mixing driven by Brownian motion. This creates multiple heat transfer pathways, significantly improving thermal conductivity and convective heat transfer. As φ increases, *Nu* increases linearly, indicating that higher nanoparticle concentrations enhance convective heat transfer. At $\varphi = 0.001$, corresponding to the base fluid without nanoparticles, *Nu* starts at a lower value. As the volume fraction increases to 0.03, Nu rises steadily, indicating that adding graphene, silver, and gold nanoparticles improves the fluid's heat transfer efficiency. This linear relationship highlights the significant role of nanoparticle concentration in enhancing thermal performance. Higher *Nu* values indicate more efficient heat transfer, which is critical for optimizing the heat exchanger's performance in industrial applications. Therefore, using the tri-hybrid nanofluid with higher nanoparticle concentrations can substantially improve the overall efficiency and energy performance of the heat exchanger system.

Increasing nanoparticle concentration improves heat transfer through enhanced thermal conductivity and micro-convection, but also increases fluid viscosity and wall shear stress, leading to higher pressure drop and increased pumping costs. Therefore, an optimal concentration balances thermal gains against hydraulic penalties in parallel-plate heat exchangers.

Finally, the augmentation of Nu with increasing Reynolds number and solid volume fraction is attributable to the combined effects of elevated thermal conductivity from highly conductive nanoparticles such as G, Ag, and Au; micro-convection driven by Brownian motion, which enhances thermal mixing; synergistic interactions among particles that establish efficient heat conduction networks; and boundary-layer thinning along with intensified convection at higher Reynolds numbers. Collectively, these mechanisms substantially improve convective heat transfer, rendering tri-hybrid nanofluids superior to conventional fluids, mono-nanofluids, and many hybrid nanofluids in thermal management applications.

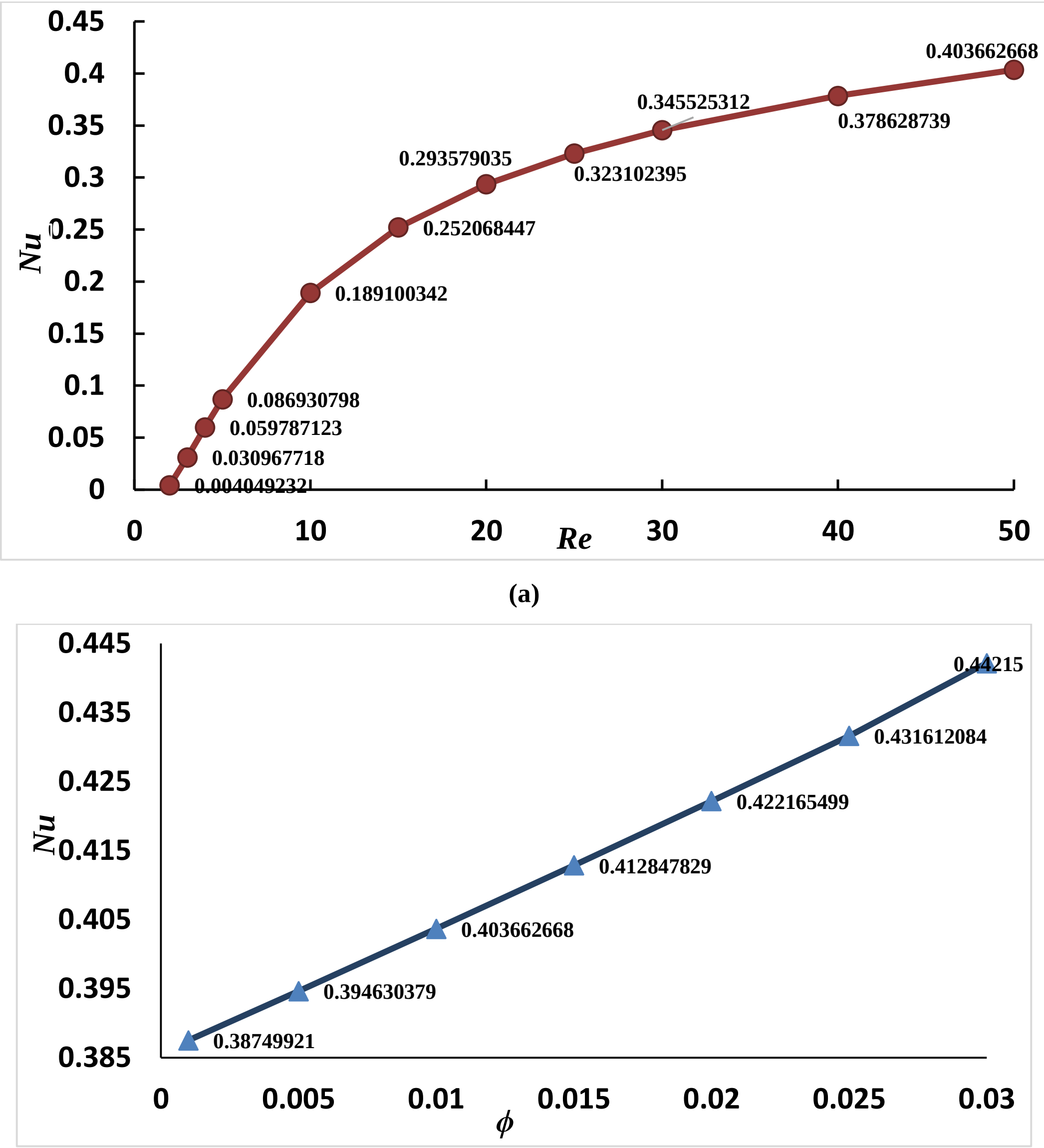

(a)

(b)

Figure 8: Average *Nu* for different (a) *Re*, and (b) ϕ.

5.4 Pressure drop

Pressure drop is the difference in fluid pressure between two points in a flow system, caused by friction, elevation changes, and flow restrictions like bends or valves. It's crucial in the design of fluid transport systems, as excessive pressure drop can lead to inefficiencies, increased energy use, and potential system failure. In this study, the pressure drop is calculated by equation (6). The graph in Figure 9 shows the connection Re-Δp in the HE when the nanoparticle volume fraction (φ) is kept constant at 0.01. As the Reynolds number increases from 0 to 50, the pressure drop increases steadily. The pressure drop is approximately 235 Pa at low Re, then gradually increases to approximately 237 Pa as the flow rate increases. This indicates that higher flow rates (higher *Re*) result in greater flow resistance, leading to a higher pressure drop in the system. The consistent rise in pressure drop with increasing Re values emphasizes the trade-off between enhanced heat transfer and increased energy costs due to higher flow resistance in the heat exchanger. Pressure drop can't be fully eliminated because it depends on flow velocity, but it can be reduced by operating at an optimal Reynolds number, maintaining low nanoparticle concentrations, ensuring stable dispersion, and using optimized heat exchanger geometries. In practice, the aim is to balance heat transfer and pumping power, with the study's operating range reflecting a compromise between thermal gain and hydraulic losses.

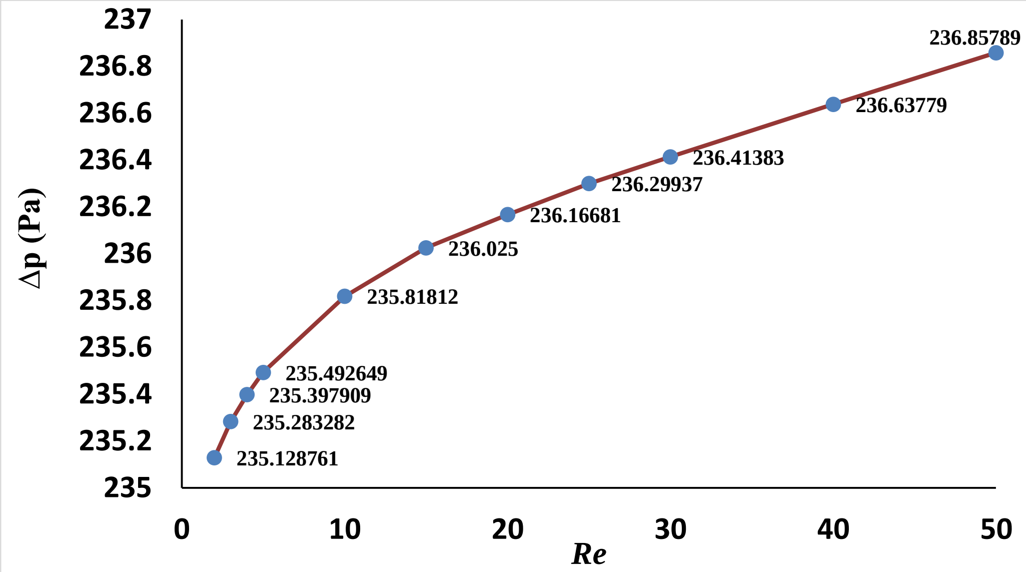

Figure 9: Pressure drop versus Reynolds number with ϕ = 1%.

5.5 Friction factor

The fanning friction factor is the ratio of wall shear stress to the fluid's dynamic pressure, as given by equation (7). Figure 10 illustrates the relationship between the fanning friction factor (f) and Reynolds number (Re) for the tri-hybrid nanofluid at a constant solid volume fraction ($\varphi = 1\%$). The Fanning friction factor, which represents the resistance to flow within the heat exchanger, is plotted on the y-axis. In contrast, the Reynolds number, a dimensionless quantity representing the ratio of inertial to viscous forces, is plotted on the x-axis. The graph shows that the Fanning friction factor decreases significantly as the Reynolds number increases. At low Reynolds numbers (Re = 2, 3, 4, 5), the Fanning friction factor is relatively high, indicating higher resistance to flow. As the Reynolds number increases to moderate values (Re = 10, 20), the friction factor decreases sharply, showing a marked reduction in flow resistance. At higher Reynolds numbers (Re = 30, 40, 50), the friction factor stabilizes, indicating minimal changes in resistance despite further increases in *Re*. This trend highlights improved flow characteristics and reduced pressure drop in the HE at higher *Re*, resulting in enhanced thermal performance and energy efficiency. The graph underscores the importance of optimizing Reynolds numbers to minimize flow resistance and improve HT efficiency in tri-hybrid nanofluid heat exchanger systems. The friction factor diminishes as the Reynolds number increases, owing to the fact that elevated Reynolds numbers signify that inertial forces surpass viscous forces. Consequently, the relative resistance from wall friction decreases, resulting in a lower friction factor, although the overall pressure drop may still increase due to higher flow velocities.

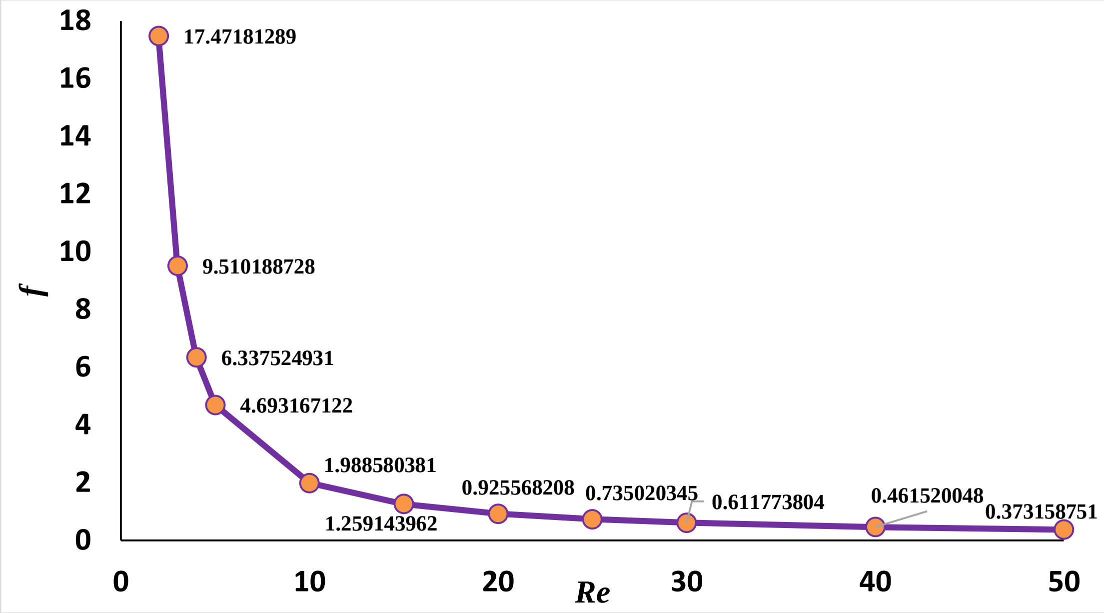

Figure 10: Fanning friction for Reynolds number variation with ϕ = 1%.

5.6 Synergy number

Synergy number indicates how well the temperature and velocity fields are aligned to optimize heat transfer. In this research, it is assessed by equation (8). The bar chart in Figure 11 illustrates the variation of the synergy number (Fc) with the Reynolds number (Re) for a tri-hybrid nanofluid at a constant solid volume fraction ($\varphi =$ 1%). The synergy number, which quantifies the interaction between the thermal and flow fields in the heat exchanger, exhibits notable trends across varying Reynolds numbers. Starting from $Re = 2$, the synergy number shows a gradual increase, indicating a strengthening interaction between the temperature and velocity fields. As the Reynolds number continues to increase, this trend persists, with the synergy number reaching its highest value at $Re = 50$, approximately 0.0007.

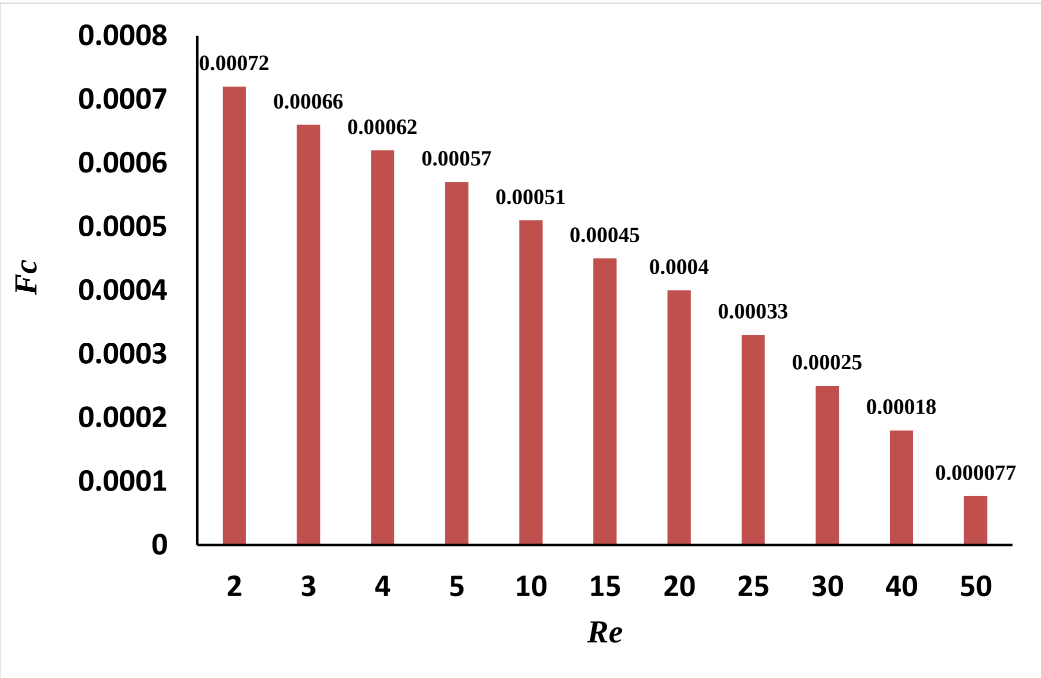

Figure 11: Synergy number as a function of Re at ϕ = 1%.

This steady rise in the synergy number suggests that higher Reynolds numbers enhance alignment between the thermal and flow fields, thereby improving heat transfer performance in the heat exchanger. This observation highlights the potential to optimize heat exchanger efficiency by operating at higher Reynolds numbers with tri-hybrid nanofluids.

The synergy number measures the coordination between velocity and temperature-gradient fields in a heat exchanger. Higher synergy indicates better alignment, boosting convective heat transfer. In the DW:EG (= 50:50) mixture-based G–Ag–Au tri-hybrid nanofluid, increasing Reynolds number and nanoparticle concentration strengthen flow-thermal interactions, raising the synergy number. This enhanced synergy improves the Nusselt number and thermo-hydraulic performance.

5.7 Pumping power

Pumping power is the energy required to move a fluid through a system, overcoming friction, pressure differences, and flow obstructions. It is a critical factor in designing efficient fluid transport systems, directly influencing operational costs and energy consumption. Pumping power was estimated by equation (10). Graph 12 illustrates the pumping power as a function of the Reynolds number (*Re*) for the tri-hybrid nanofluid with a nanoparticle volume fraction (φ) of 0.01. As *Re* increases from 0 to 50, pumping power also increases, indicating a direct relationship between flow rate and pumping power in the heat exchanger. The pumping power increases gradually at lower *Re* values, suggesting relatively lower energy consumption for fluid movement. As *Re* exceeds 10, the pumping power increases steadily, indicating a consistent increase in the energy required to maintain fluid flow at higher Reynolds numbers. This trend reflects the linear relationship between the flow rate and the energy needed to pump the fluid through the heat exchanger. Overall, the graph shows that even at a low nanoparticle concentration (ϕ = 0.01), pumping power increases clearly with increasing Reynolds number. This is crucial for understanding the energy requirements and optimizing the design of the heat exchanger system using the tri-hybrid nanofluid.

At moderate Reynolds numbers, heat transfer often outpaces the increase in pumping power, keeping the system efficient. For industrial systems such as heat exchangers, solar collectors, electronic cooling, and chemical units, tri-hybrid nanofluids are viable when the increase in Nusselt number greatly exceeds the increase in pump power. While higher Reynolds numbers and nanoparticle concentrations boost heat transfer, practical use requires balancing thermal benefits with pumping energy costs to maintain system efficiency and economic viability. Increasing the Reynolds number enhances convective heat transfer and thins thermal boundary layers, but it also increases pressure losses and pump demands. Overall performance depends on weighing heat transfer gains against hydraulic penalties.

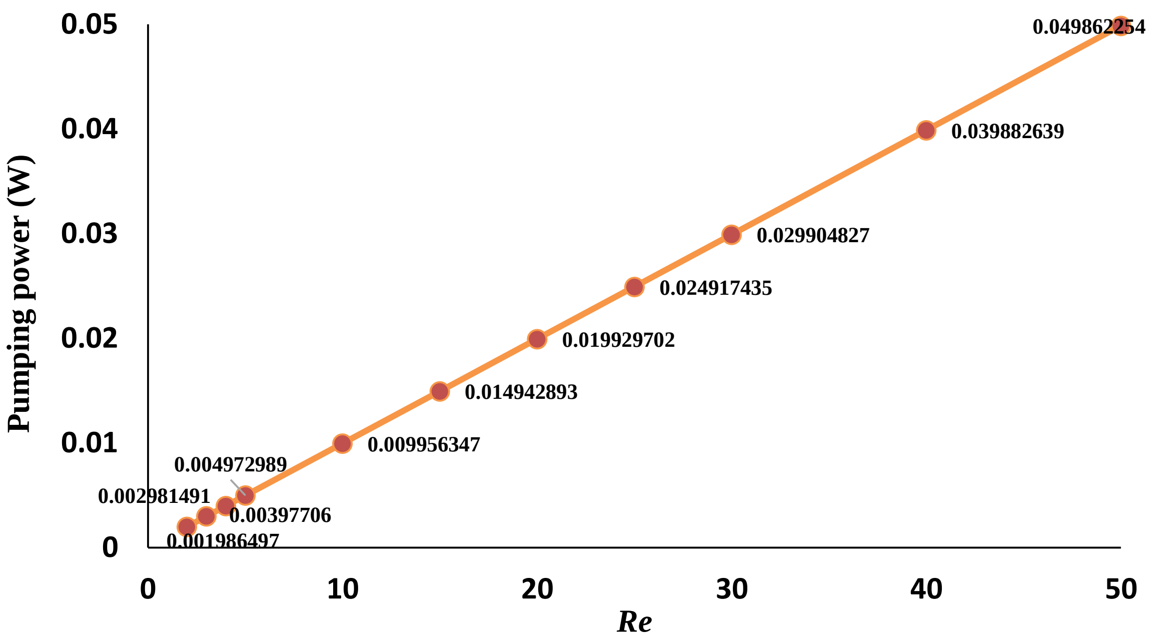

Figure 12: Pumping power against Reynolds number with ϕ = 1%.

5.8 Thermal efficiency

Thermal efficiency is a measure of how effectively a system converts heat energy into useful work or output, typically expressed as a percentage of the total energy input, and is calculated by the equation (11). Graph 13 depicts the thermal enhancement efficiency (ε) as a function of the Reynolds number (*Re*) for the tri-hybrid nanofluid with a nanoparticle volume fraction of 1%. As Re increases from 0 to 50, the thermal efficiency decreases, indicating the relationship between the flow rate and the HT enhancement in the heat exchanger. At lower *Re* values, the thermal enhancement efficiency approaches 1, demonstrating the significant effectiveness of the tri-hybrid nanofluid in improving thermal performance at low flow rates. As *Re* exceeds 10, the efficiency decreases gradually, stabilizing at 0.4-0.5 at higher *Re* values. This trend reflects the nanofluid's sustained performance even at higher flow rates. Overall, the graph strongly supports using a 1% trihybrid nanofluid concentration, demonstrating its capability to enhance thermal efficiency across a wide range of Reynolds numbers, which is crucial for optimizing the design and performance of heat exchanger systems.

Although thermal efficiency indicates heat transfer, it doesn't account for hydraulic losses. The performance index provides a more comprehensive evaluation by accounting for heat-transfer improvements and pressure-drop penalties. Thus, it is considered a more meaningful criterion for assessing the overall effectiveness and practicality of nanofluid-based heat exchangers.

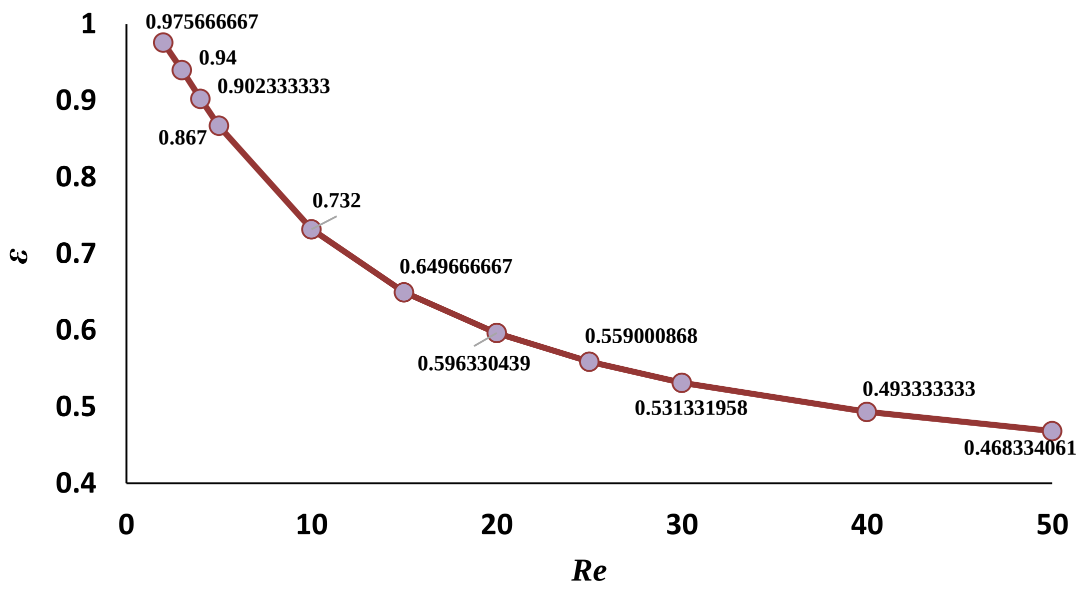

Figure 13: The thermal enhancement efficiency for different *Re* with ϕ = 1%.

5.9 Performance index

The hydraulic performance index assesses the balance between energy input and desired performance outcomes. The hydraulic performance index (η) graph calculated from equation (13) (which is unitless) is shown in Figure 14 as a function of the Reynolds number (*Re*) for the trihybrid nanofluid with a nanoparticle volume fraction ($\varphi =$ 1%).

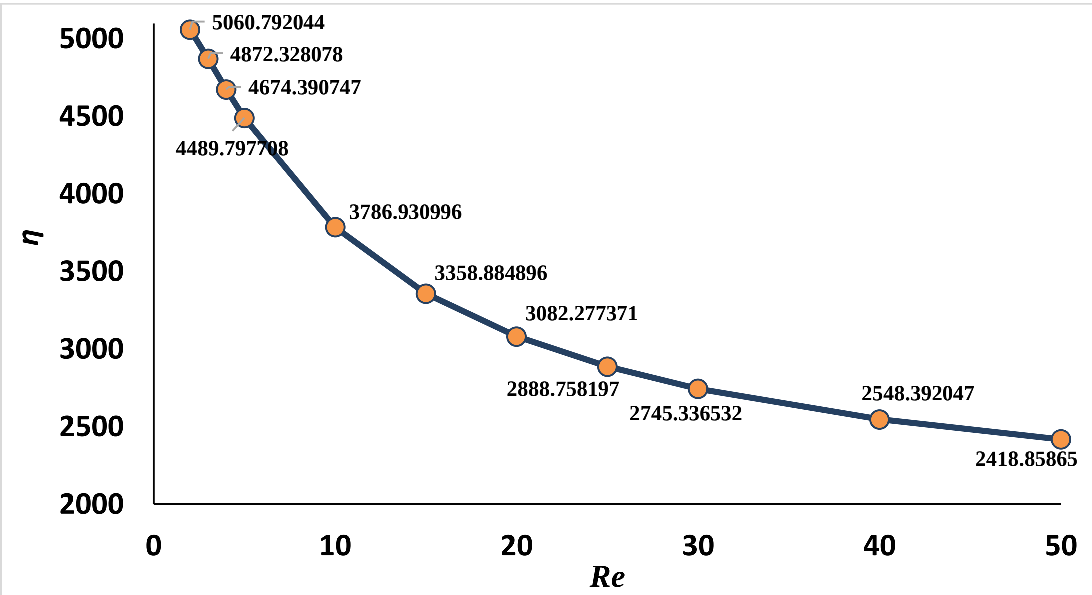

Figure 14: Hydraulic performance index versus *Re* with ϕ = 1%.

As *Re* increases from 0 to 50, the performance index decreases, indicating a relationship between the flow rate and the heat exchanger's overall performance. At low *Re* values, the performance index is exceptionally high, around 5000, highlighting the significant enhancement of the tri-hybrid nanofluid at lower flow rates. This demonstrates the nanofluid's capability to substantially improve heat exchanger performance in scenarios where lower flow rates are preferred. As *Re* increases from 0 to 20, the performance index decreases gradually to approximately 3000, suggesting that, while performance enhancement diminishes, it remains notably higher than that of conventional fluids. Beyond Re = 20, the performance index declines more slowly, stabilizing around 2000 at higher Re values, indicating that the trihybrid nanofluid maintains significant efficiency benefits even at higher flow rates. Overall, this graph supports using a 1% tri-hybrid nanofluid concentration, demonstrating its robust performance enhancement across various flow rates, which is crucial for optimizing the efficiency and effectiveness of heat exchanger systems.

5.10 Fluid temperature

Graph 15 shows how the working fluid temperature changes along the centerline of a counterflow heat exchanger channel, with the x-axis indicating length in millimeters and the y-axis showing temperature in Kelvin. The blue line represents the hot channel temperature. Initially, the temperature is around 315 K at 0 mm. As the fluid travels through the channel, its temperature gradually increases, reaching approximately 320 K at 250 mm. This trend indicates that the hot fluid consistently transfers heat along its path. The orange line depicts the average cold channel temperature. Starting at about 300 K at the 0 mm mark, the temperature rises steadily along the channel length, reaching around 315 K at the 250 mm mark. This increase demonstrates that the cold fluid absorbs heat efficiently as it moves through the channel. These temperature profiles effectively demonstrate the heat exchange process in the counterflow configuration. The hot fluid transfers heat to the cold fluid as it flows in opposite directions, increasing the cold fluid's temperature and decreasing the hot fluid's temperature. The gradual, continuous temperature change along the channel length highlights the heat exchanger system's efficient thermal performance, ensuring effective heat transfer between the fluids.

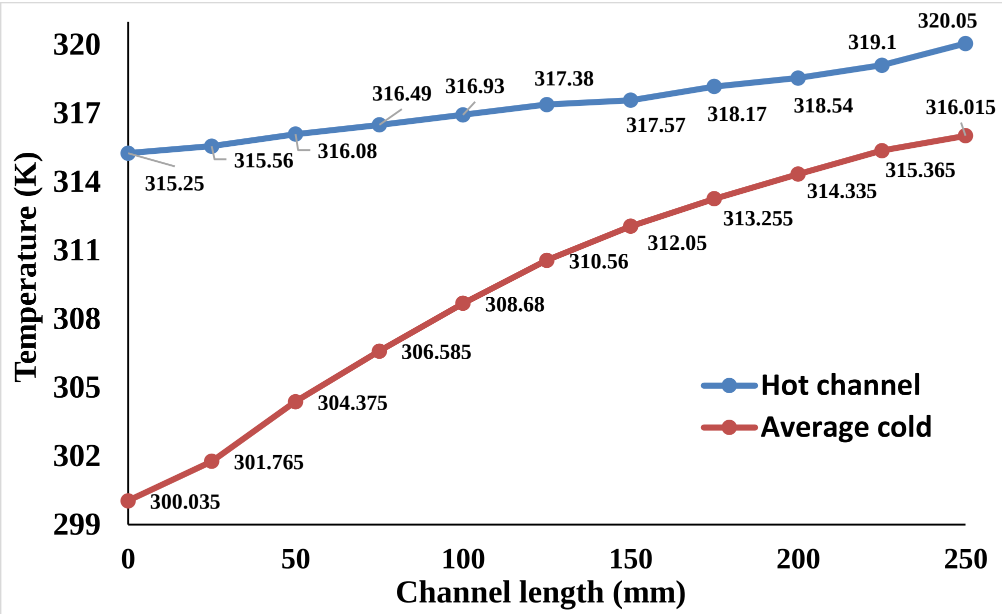

Figure 15: Fluid temperature variations at different positions along the middle line of the channel.

5.11 Comparison

The comparison of the present study with Hasan et al. (2009) in terms of thermal enhancement efficiency (ε) and thermal performance index (η*) (1/Pa) calculated from equation (12), whose unit is (1/Pa), demonstrates the superior performance of the current research in Figure 16. In the thermal enhancement efficiency (ε) plot, the present study shows higher initial values than those of Hasan et al. (2009), starting around 0.7, whereas Hasan et al.'s (2009) values are approximately 0.68. This indicates greater thermal enhancement at low Reynolds numbers (Re). Both studies exhibit a decline in ε as Re increases. Still, for Re values between 50 and 200, the present research reports slightly higher ε values, ranging from around 0.4 to 0.2, compared to Hasan et al.'s drop to approximately 0.35-0.15. The present study consistently shows an advantage in the mid-range Re values (200 to 600), with ε values around 0.2 compared to Hasan et al.'s 0.15. Both studies show a further decline and stabilization at higher Re values (600-1000). Still, the present study shows slightly better ε, approximately 0.12, compared to Hasan et al.'s approximate value of 0.1.

The thermal performance index (η*) (1/Pa) plot provides a comparative analysis between the present study and Hasan et al. (2009), showing notable differences across varying Reynolds numbers (Re). At low Re values, the performance index in the current research begins at approximately 0.006, slightly higher than Hasan et al.'s starting point of around 0.0055. As Re increases, both studies observe a steep decline in η*, but the drop in the present study is more gradual, reaching about 0.0015 at Re = 100, compared to Hasan et al.'s sharper decrease to approximately 0.001. In the mid-range Re values (100 to 500), the present study consistently maintains a higher performance index, stabilizing around 0.001, while Hasan et al.'s values level off closer to 0.0008, indicating better overall performance in this range. At higher *Re* values (500-1000), both studies show a further flattening of the trend. Still, the present study continues to demonstrate a slight advantage, with η^* remaining around 0.0006, compared to Hasan et al.'s value of 0.0005. This broader analysis highlights the superior performance and efficiency of the tri-hybrid nanofluid in enhancing HE thermal performance across a wide range of flow conditions.

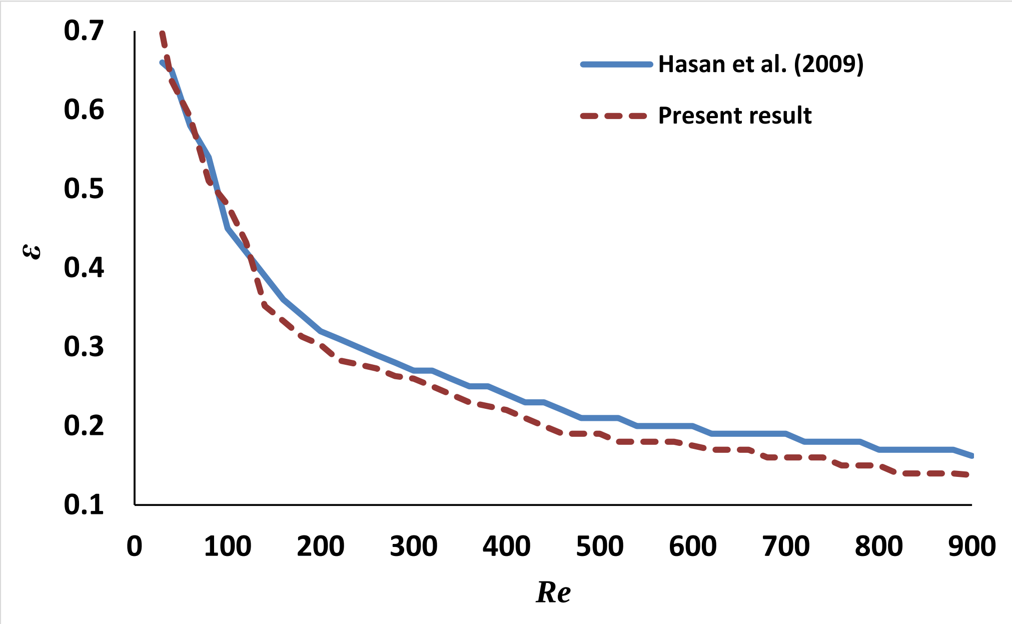

(a)

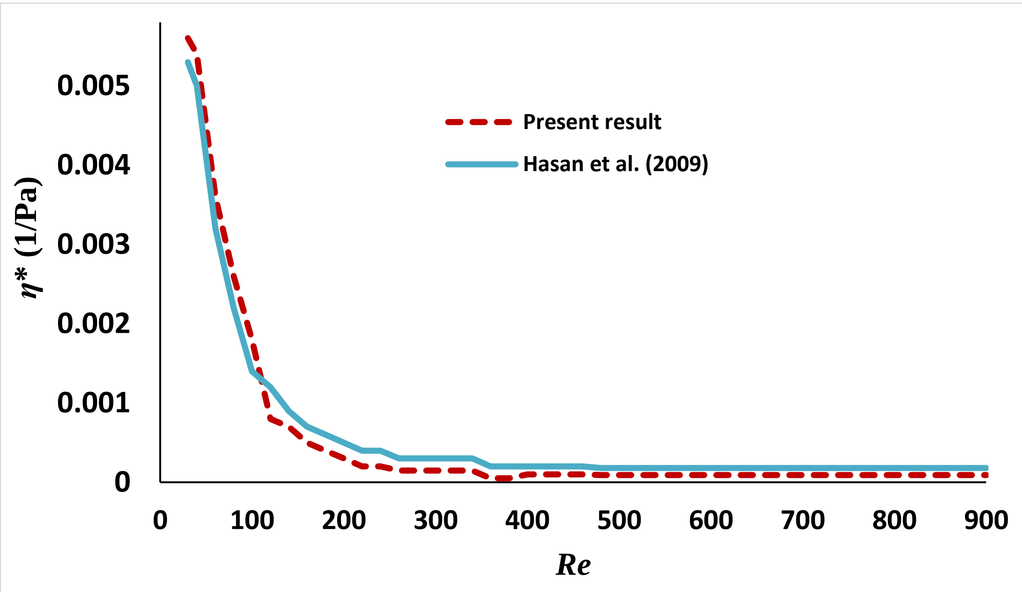

(b)

Figure 16: Comparison of the present study with Hasan et al. (2009) in terms of (a) thermal enhancement efficiency (ε), and (b) thermal performance index (η^*)

6. Major Outcomes

The major outcomes are as follows:

- The average Nusselt number (Nu) increases by about 70% as Re increases from 0 to 50 and by 14.10% as the nanoparticle volume fraction increases from 0 to 0.03, reflecting improved heat transfer at higher concentrations.

- ❖ The total pressure drop increases by roughly 0.74% as Re varies from 0 to 50 at $\phi = 0.01$, showing a trade-off between better heat transfer and increased pressure drop.
- ❖ The pumping power increases linearly from 0 W to about 0.05 W as Re rises from 0 to 50, a 2410.06% increase, showing a direct link between flow rate and energy use in the heat exchanger.
- ❖ The synergy number (Fc) increases by 800% from Re 2 to 50, indicating improved heat transfer efficiency with the tri-hybrid nanofluid at higher Re.
- ❖ The thermal enhancement efficiency (ε) in this study surpasses that of Hasan et al. [7] by up to 25%, especially at lower Reynolds numbers, highlighting the superior thermal properties of the tri-hybrid nanofluid.
- ❖ The temperature profile shows a 2% drop in hot fluid temperature and a 5% rise in cold fluid temperature, indicating effective heat transfer.

Thus, the optimum flow conditions for this research are a Reynolds number of 5 and a solid volume fraction of 1%. This study shows that tri-hybrid nanofluids enhance heat transfer by increasing convective coefficients and thermal conductivity. An optimized heat exchanger with steel plates and three chambers improves heat transfer, while advanced methods more accurately assess performance. These advances could lead to smaller, more efficient heat exchangers that use less energy. The findings support the use of tri-hybrid nanofluids, which enhance thermal performance across a range of flow rates and concentrations. Overall, they offer significant benefits over conventional fluids and earlier research, making them a promising choice for heat exchanger efficiency.

6.1 Applicability to real systems

The developed FEM model is assumed to be representative of practical thermal systems operating under comparable flow and thermal conditions. The selected Reynolds number range, nanoparticle concentrations, and boundary conditions are intended to reflect realistic engineering applications. Although certain practical factors, such as fouling, nanoparticle sedimentation, surface roughness, and equipment degradation, are neglected, the model still provides a realistic approximation of the thermo-hydraulic performance of tri-hybrid nanofluid-based heat exchangers and related thermal management systems.

6.2 Limitations

Despite substantial progress in thermal efficiency, the practical deployment of tri-hybrid nanofluids remains limited by challenges including long-term dispersion stability, elevated material costs, increased pumping power requirements, and the potential for erosion and fouling. These considerations must be carefully weighed against the benefits of heat transfer to evaluate their suitability in actual industrial applications.

6.3 Future research

- ❖ Eco-friendly fluids such as bio-glycols, vegetable oils, or ionic liquids may offer sustainable thermal management options.
- ❖ The analysis could include complex geometries like corrugated, wavy, finned, microchannel, and multi-pass heat exchangers for tri-hybrid nanofluids.
- ❖ Thermodynamic assessments, such as entropy minimization and exergy analysis, can deepen understanding of irreversibilities.
- ❖ Data-driven models and machine learning can accurately predict properties and optimal conditions with less computational cost.
- ❖ The economic viability of noble-metal nanoparticles like silver and gold should consider synthesis, maintenance, and environmental impacts.
- ❖ The performance under transient conditions, turbulence, and variable heat loads must be investigated for industrial applications.

References

Alatawi, E.S., Sannyashi, B., Nasrin, R., Ferdoushi, Most. Z., and Feng, Z.-G. (2025): Efficiency enhancement of a cone-column combined microchannel heat sink featuring graphene-water nanofluid, Energies, 18, 1727, https://doi.org/ 10.3390/en18071727.

Ali, S., Shaiq, S., Shahzad, A., Sohail, M., Naseem, T. (2024): Numerical thermal investigation of radiative magnetohydrodynamics axisymmetric Cu-Al_2O_3/H_2O hybrid nanofluid flow over an unsteady radially stretched surface, International Journal of Ambient Energy, 45(1), 2321210.

Arasteh, H., Mashayekhi, R., Ghaneifar, M., Toghraie, D., Afrand, M. (2019): Heat transfer enhancement in a counter-flow sinusoidal parallel-plate heat exchanger partially filled with porous media using metal foam in the channels' divergent sections, Journal of Thermal Analysis and Calorimetry, 141, 1669–1685, https://doi.org/10.1007/s10973-019-08870-w

Barzegarian, R., Moraveji, M. K., Aloueyan, A. (2016): Experimental investigation on heat transfer characteristics and pressure drop of BPHEx (brazed plate heat exchanger) using TiO_2–water nanofluid, Experimental Thermal and Fluid Science, 74, 11-18, https://doi.org/10.1016/j.expthermflusci.2015.11.018

Brinkman, H.C. (1952): The viscosity of concentrated suspensions and solution, Journal of Chemical Physics, 20, 571-581, https://doi.org/10.1063/1.1700493

Elsaida, K., Abdelkareemb, M.A., Maghrabiee, H.M., Sayedc, E.T., Wilberforcef, T., Baroutajig, A., Olabi, A.G. (2021): Thermophysical properties of graphene-based nanofluids, International Journal of Thermofluids, 10, 100073, https://doi.org/10.1016/j.ijft.2021.100073

Galeazzo, F.C.C., Miura, R.Y., Gut, J.A.W., Tadini, C.C. (2006): Experimental and numerical heat transfer in a plate heat exchanger, Chemical Engineering Science, 61, 7133 – 7138, https://doi.org/10.1016/j.ces.2006.07.029

Garnett, J.C.M. (1904): Colours in metal glasses and in metallic films, Royal Society, 203, 85-420.

Gherasim, I., Taws, M., Galanis, N., Nguyen, C.T. (2011): Heat transfer and fluid flow in a plate heat exchanger part I. Experimental investigation, International Journal of Thermal Sciences, 50, 1492-1498, https://doi.org/10.1016/j.ijthermalsci.2011.03.018

Govindasamy, S., Mebarek-Oudina, F., Harikrishnan, S., Swaminathan, C., Gundagnai, M., Krishna, R., Alkateb, H., Vaydia, H. (2026): Experimental and machine-learning investigation of ZnO nanofluid flow in a triangular-absorber parabolic trough collector, Modern Physics Letters B, 40(15), https://dx.doi.org/10.1142/S0217984926501083

Guo, K., Zhang, N., Smith, R. (2015): Optimisation of fin selection and thermal design of counter-current plate-fin heat exchangers, Applied Thermal Engineering, 78, 491-499, http://dx.doi.org/10.1016/j.applthermaleng.2014.11.071

Hasan, M.I. (2011): Numerical investigation of counter flow microchannel heat exchanger with MEPCM suspension, Applied Thermal Engineering, 31, 1068-1075, https://doi.org/10.1016/j.applthermaleng.2010.11.032

Hasan, M.I., Rageb, A.A., Yaghoubi, M., Homayoni, H. (2009): Influence of channel geometry on the performance of a counter flow microchannel heat exchanger, International Journal of Thermal Sciences, 48, 1607–1618, https://doi.org/10.1016/j.ijthermalsci.2009.01.004

Hong, F., Cheng, P. (2009): Three dimensional numerical analyses and optimization of offset strip-fin microchannel heat sinks, International Communications in Heat and Mass Transfer, 36, 651–656, https://doi.org/10.1016/j.icheat masstransfer.2009.02.01

Jahan, S. and Nasrin, R. (2025): Sensitivity study of thermal enhancement featuring ternary-hybrid nanofluid in a two-layered cross-flow microchannel heat exchanger, Journal of Thermal Analysis and Calorimetry, 150, 17591–17616, https://doi.org/10.1007/s10973-025-14568-z

Jahan, S. and Nasrin, R. (2026): Predictive ANN analysis of hydrothermal and entropy behavior of corrugated heat exchanger featuring tetra-hybrid nanofluid, South African Journal of Chemical Engineering, 56, 439-459, https://doi.org/10.1016/j.sajce.2025.12.012

Jahan, S., Nasrin, R., Biswas, C., and Ferdoushi, Most. Z. (2025): Sensitivity study for performance evaluation criterion of a crossflow microchannel heat exchanger using response surface model, International Journal of Ambient Energy, 46(1), 2507142, 2025, https://doi.org/10.1080/01430750.2025.2507142

Kikic, M.S., Knezevic, K.G., Vranic, M.J., Trivic, M.S. (2021): Influence of the number of transfer units on heat transfer in a cross-flow plate heat exchanger. Thermal Science, 25(1), 425-438.

Li, M., Li, H., Li, X., Li, Y. (2021): Heat transfer and friction characteristics of a plate heat exchanger with novel curved plates. Applied Thermal Engineering, 186, 387-395.

Marra, F., Raganati, F., Tola, A., Iaquaniello, G., Albano, L. (2021): Design optimization of plate heat exchangers for waste heat recovery. Energy Conversion and Management, 234, 113760.

Mebarek-Oudina, F., Bouselsal, M., Khan, S.U., Ramesh, K., Ismail, A.I. (2025): Optimizing thermal performance in shell-and-tube heat exchangers with tri-hybridised nanofluids: a numerical study of turbulent convection, Thermal Science and Engineering Progress, 65, 103988, https://doi.org/10.1016/j.tsep.2025.103988

Mezaache, A., Mebarek-Oudina, F., Vaidya, H., Fouad, Y. (2024): Heat transfer analysis of nanofluid flow with entropy generation in a corrugated heat exchanger channel partially filled with porous medium, Heat Transfer, 53(8), 4625-4647, https://doi.org/10.1002/htj.23149

Muhammad, A., Bhaskaran, G., Shuaib, N.H., Abu-Mulaweh, H.I. (2011): Influence of nanofluids on parallel flow square microchannel heat exchanger performance, International Communications in Heat and Mass Transfer, 38(1), 1–9, https://doi.org/10.1016/j.icheatmasstransfer.2010.09.007

Nagapavani, M., Reddy, G.V.R., Abdulrahman, A., Kumar, R., Gowda, R.J.P. (2024): Three-dimensional swirling flow of a ternary composite nanofluid induced by the torsional motion of a cylinder considering non-Fourier law, Numerical Heat Transfer, Part A: Applications, 85(13), 2183-2196.

Naseem, T., Mebarek-Oudina, F., Shahzad, A., Fish, H., Ben Hamida, M.B. (2025) : Enhanced thermodynamic irreversibility and heat transfer in rotating graphene oxide–water nanofluids over a stretching surface, Modern Physics Letters B, 40(3), https://doi.org/10.1142/s0217984925502677

Oliveira, A.C.C., Marques, A.D.A.R., Da Silva, R.C., Borges, L.H., Silva, R.M.M. (2021): Exergoeconomic analysis of a milk pasteurization plant using a plate heat exchanger. Energy Reports, 7, 3553-3558.

Ordonez, J.C., Bejan, A. (2000): Entropy generation minimization in parallel-plates counter flow heat exchangers, International Journal of Energy Research, 24, 843-864, https://doi.org/10.1002/1099-114X(200008)24:10<843::AID-ER620>3.0.CO;2-M

Peng, X.F., Wang, B.X., Peterson, G.P., Ma, H.B. (1995): Experimental investigation of heat transfer in flat plates with rectangular microchannels, International Journal of Heat and Mass Transfer, 38, 127-137, https://doi.org/10.1016/0017-9310(94)00136-J

Rao, T.S., Babu, M.M., Bojja, R.R., Santoshi, N.P., Reddy, G.V.R. (2024): Thermal radiation effects on MHD Casson and Maxwell nanofluids over a porous stretching surface, Passer Journal of Basic and Applied Sciences, 6 (1), 171-178.

Sohail, M., Waseem, F., Abodayeh, K., Rafique, E. (2025): Analysis of entropy generation on Darcy-Forchheimer squeezed hybrid nanofluid flow between two parallel rotating disks by considering thermal radiation and viscous dissipation, Numerical Heat Transfer Fundamentals 87(1), 1-23, https://doi.org/10.1080/10407790.2024.2391501

Sundar, L.S., Ramana, E.V., Singh, M.K., Sousa, A.C.M. (2014): Thermal conductivity and viscosity of stabilized ethylene glycol and water mixture Al_2O_3 nanofluids for heat transfer applications: An experimental study, International Communications in Heat and Mass Transfer, 56, 6–95,

http://dx.doi.org/10.1016/j.icheatmasstransfer.2014.06.009

Tiwari, K., Ghosh, P., Sarkar, J., Dahiya, H., Parekh, J. (2014): Numerical investigation of heat transfer and fluid flow in plate heat exchanger using nanofluids, International Journal of Thermal Sciences, 85, 93-103, https://doi.org/10.1016/j.ijthermalsci.2014.06.015

Uddin, M.J., Nasrin, R., and Alatawi, E.S. (2025): Augmenting thermal-material transport in boundary-layer flow over an upright sheet: An explicit finite difference approach, Journal of Naval Architecture and Marine Engineering, 22(1), 21-40, https://doi.org/10.3329/jname.v22i1.77636

Wang, S., Chen, L., Zhang, B., Yang, Y., Wang, X. (2020): A new design of double-layered microchannel heat sinks with wavy microchannels and porous-ribs, Journal of Thermal Analysis and Calorimetry, 141, 547–558, https://doi.org/10.1007/s10973-020-09317-3

Waseem, F., Sohail, M., Singh, A. (2023): Entropy analysis of three-dimensional stretched magnetized hybrid nanofluid with thermal radiation and heat generation, BioNanoScience, 14(2):1-19, https://doi.org/10.1007/s12668-023-01267-y

Yuan, S., Leng, Y., Fouly, A., Awwad, E.M., Nazir, U., Sohail, M. (2024): A study of four-phase fluid and thermal enhancement based on tetra-hybrid nanofluid considering temperature jump on a spinning sphere, Case Studies in Thermal Engineering, 58, 104353.

Zahan, I., Nasrin, R., and Jakia, N.J. (2025): Data analysis for performance index of plate heat exchanger filled by ionanofluid-oil: Parallel versus counter flow, Scientific Reports, 15, 4688, https://doi.org/10.1038/s41598-025-88851-2

Zahan, I., Nasrin, R., Khatun, S. (2022): Thermal performance of ternary-hybrid nanofluids through a convergent-divergent nozzle using distilled water-ethylene glycol mixtures, 137, 106254, https://doi.org/10.1016/j.icheatmasstransfer.2022.106254

Zheng, W., Sun, J., Ma, C., Yu, Q., Zhang, Y., Niu, T. (2021): Numerical study of fluid flow and heat transfer characteristics in a cone-column combined heat sink, Energies, 14, 1605, https://doi.org/10.3390/en14061605

Zhu, Q., Xia, H., Chen, J., Zhang, X., Chang, K., Zhang, H., Wang, H., Wan, J., Jin, Y. (2021): Fluid flow and heat transfer characteristics of microchannel heat sinks with different groove shapes, International Journal of Thermal Sciences, 161, 106721, https://doi.org/10.1016/j.ijthermalsci.2020.106721

Zienkiewicz, O.C., Taylor, R.L. (1991): The Finite Element Method, Fourth Edition, McGraw-Hill.